

White paper on EUSO-SPB2

James H. Adams Jr.,¹ Luis A. Anchordoqui,^{2,3} Jeffrey A. Apple,⁴ Mario E. Bertaina,⁵
 Mark J. Christl,⁴ Francesco Fenu,⁵ Evgeny Kuznetsov,¹ Andrii Neronov,⁶
 Angela V. Olinto,⁷ Etienne Parizot,^{8,9} Thomas C. Paul,² Guillaume Prévôt,⁸
 Patrick Reardon,¹ Ievgen Vovk,¹⁰ Lawrence Wiencke,¹¹ and Roy M. Young⁴

¹*Center for Space Plasma and Aeronomic Research,
 University of Alabama in Huntsville, Huntsville, AL 35899, USA*

²*Department of Physics & Astronomy,
 Lehman College, City University of New York, NY 10468, USA*

³*Department of Astrophysics, American Museum of Natural History, NY 10024, USA*

⁴*Marshall Space Flight Center, Huntsville, AL 35812, USA*

⁵*Dipartimento di Fisica, Università di Torino, Torino, Italy*

⁶*Astronomy Department,
 University of Geneva, Ch. d'Ecogia 16, 1290, Versoix, Switzerland*

⁷*Department of Astronomy & Astrophysics,
 Enrico Fermi Institute and Kavli Institute for Cosmological Physics,
 University of Chicago, Chicago, IL 60637, USA*

⁸*Université Paris Diderot, Laboratoire Astro Particule et Cosmologie, CNRS, Paris, France*

⁹*Observatoire de Paris, Sorbonne Paris Cité, 119 75205 Paris, France*

¹⁰*Max Planck Insitut fur Physik, Foehringner Ring 6, 80805, Munich, Germany*

¹¹*Department of Physics, Colorado School of Mines, Golden, CO 80401, USA*

Abstract

EUSO-SPB2 is a second generation Extreme Universe Space Observatory (EUSO) on a Super-Pressure Balloon (SPB). This document describes the physics capabilities, the proposed technical design of the instruments, and the simulation and analysis software.

Contents

I. SCIENCE OBJECTIVES	3
A. General idea	3
B. Observational status of high- and ultrahigh-energy cosmic rays	4
C. Properties of nearly horizontal air showers developing at high altitude	8
D. The hunt for astrophysical tau-neutrinos using upgoing air showers	9
E. Cosmic ray physics using Cherenkov light	10
F. NASA's POEMMA	11
II. TECHNICAL DESIGN OF THE INSTRUMENTS	12
A. Observation and measurement strategies	12
B. Integrated gondola	16
1. Overview	16
2. Pointing control	16
3. Power system	18
4. Telemetry	19
C. Optics design	20
D. Focal plane detectors	23
1. Muon Cherenkov sensor	23
2. Upward directed Cherenkov signals	26
3. Fluorescence sensor	26
4. Infrared camera	27
5. Testing plans	27
6. Advanced sensor development	27
7. Mission operations	28
III. SIMULATION AND ANALYSIS SOFTWARE	28
A. <u>Offline</u> design	30
B. ESAF design	32
C. Use of <u>Offline</u> and ESAF for EUSO pathfinders	33
D. EUSO-SPB2	36
IV. EXPECTED PERFORMANCE	37
A. Duty cycle	37
B. Event rates	38
1. Estimate of UHECR events using ESAF	38
2. Estimate of UHECR event rates using CONEX + <u>Offline</u>	38
V. DEVELOPMENT SCHEDULE AND DATA MANAGEMENT	41
References	42

I. SCIENCE OBJECTIVES

A. General idea

We propose to monitor the night sky of the Southern hemisphere with a second generation of the Extreme Universe Space Observatory (EUSO) instrument, to be flown aboard a Super-Pressure Balloon (SBP). This mission, EUSO-SPB2, has several exploratory and scientific objectives.

EUSO-SPB2 will be the first instrument to measure air-showers by viewing their Cherenkov light from high in the atmosphere. We expect to observe a rather large sample of cosmic rays in the energy range $10^7 \lesssim E/\text{GeV} \lesssim 10^8$, with the aim of discriminating among primary protons, heavy nuclei, and photons via their characteristic Cherenkov profiles [1]. The instrument will also be able to characterize the background for upward going showers initiated by the decay of tau leptons which are expected to be produced by Earth-skimming tau neutrinos [2].

In addition to detection of Cherenkov light, we plan to use fluorescence light from air showers to measure, for the first time, the evolution of nearly horizontal extensive air showers, which develop at high altitude in a nearly constant density atmosphere. Such measurements will provide a unique channel to tune hadronic interaction models at ultra-high energies, and may elucidate the reason why ultrahigh-energy cosmic ray (UHECR) showers observed by ground-based detectors contain more muons than expected from existing hadronic interaction models [3].

Importantly, EUSO-SPB2 will serve as a pathfinder for the more ambitious space-based measurements by the Probe Of Extreme Multi-Messenger Astrophysics (POEMMA), selected by NASA for an in-depth probe mission concept study in preparation for the next decadal survey. POEMMA will combine the well-developed Orbiting Wide-field Light-collectors (OWL) concept [4] with the recently proposed Cherenkov from Astrophysical Neutrinos Telescope (CHANT) concept [2] to form a multi-messenger probe of the most extreme environments in the universe.

EUSO-SPB2 will build upon the experience of flying EUSO-SPB in the Spring of 2017. A number of upgrades will render EUSO-SPB2 more powerful, including a Schmidt design reflecting telescope and a faster ultraviolet (UV) camera to increase exposure to UHECR observations. The new instrument will detect the fluorescence signal from UHECR generated air-showers of highly inclined events. EUSO-SPB2 will be built to view the true horizon of the Earth. Horizontal observations will lead to much larger acceptances for inclined UHECRs, with a distance-dependent energy threshold. We are also prepared to consider additional nadir observations of the fluorescence based on EUSO-SPB results. The combination of nadir (EUSO-SPB) and tilted (EUSO-SPB2) observations will explore the power of space observatories to observe UHECR of extreme energies. A long enough flight of EUSO-SPB2 observations will match and complement ground observations [5].

In addition to improving the exposure to UHECRs, EUSO-SPB2 will study the possibility of detecting tau neutrinos via direct Cherenkov light [2]. A coincidence veto will be developed for EUSO-SPB2 so it can characterize the background for Cherenkov signals

from the decay of tau leptons, produced in charged current interactions of Earth skimming neutrinos. EUSO-SPB2 will inform the best strategy for future space missions such as POEMMA.

The detectors aboard EUSO-SPB2 will measure the Cherenkov signals from nearly horizontal air-showers initiated by high-energy cosmic rays in the upper atmosphere. The instrument will use the technique of imaging atmospheric Cherenkov telescopes (IACT), which is widely used in contemporary gamma-ray astronomy. We expect a large statistical sample which will allow for study of spectral features and composition in an interesting energy regime. Since good distinguishing power between baryon and photon induced showers has been shown to be feasible for an IACT [1] we can theoretically reach a competitive photon sensitivity with a similar airborne instrument.

EUSO-SPB2 addresses the fourth science goal of the 2011 NASA Strategic Plan [6], to “Discover how the universe works, explore how it began and evolved” and one of the “Physics of the Cosmos” questions in NASA’s 2010 Science Plan [7]: “How do matter, energy, space, and time behave under the extraordinarily diverse conditions of the cosmos?” EUSO-SPB2 directly addresses the sixth question in the Connecting Quarks with the Cosmos report [8] in this report’s list of “Eleven Science Questions for the New Century,” which is “How do Cosmic Accelerators Work and What are They Accelerating?” EUSO-SPB2 science is in line with the NASA Astrophysics Roadmap of 2013 missions for the next 3 decades [9]. Upcoming measurements of EUSO-SPB2 are essential to achieve the ambitious recommendations of the U.S. HEP Snowmass planning process: “The Bright Side of the Cosmic Frontier: Cosmic Probes of Fundamental Physics” [10].

B. Observational status of high- and ultrahigh-energy cosmic rays

The origin(s) of cosmic rays remains a challenging enigma of particle astrophysics. The energy spectrum is known to span about eleven decades of energy, $1 \lesssim E/\text{GeV} \lesssim 10^{11}$. The spectral shape can be described by a broken power law with three major breaks: the steepening of the spectrum dubbed the “knee” at $E \approx 10^{6.6}$ GeV [11], a pronounced hardening of the spectrum at $E \approx 10^{9.6}$ GeV, the so-called “ankle” feature [12–14], and the high frequency cutoff at $E \approx 10^{10.6}$ GeV [14, 15]. Three additional more subtle features have been reported over the years in between the knee and the ankle: a hardening of the spectrum at $10^{7.3}$ GeV [16–19] followed by two softenings at $10^{7.9}$ GeV [16, 17] and $10^{8.5}$ GeV [18–21]. The latter softening is usually referred to as the “second knee.”

The variations of the spectral index in the energy spectrum reflect various aspects of cosmic ray production, source distribution, and propagation. The first and the second knee reflect characteristic energy scales of magnetic confinement and/or acceleration capability of the sources, both of which grow linearly in the charge Z of the nucleus. The first knee has been studied by a number of experiments and its characteristics are well represented by magnetic rigidity effects for different nuclear composition [22]. The physical significance of the second-knee, however, is less well established and the energy at which the Galactic extragalactic transition takes place is an open question.

From existing IACT data, we can estimate the EUSO-SBP2 sensitivity to high-energy

cosmic ray events. If we assume a trigger threshold of 100 photoelectrons with 100 days of data collection, we find that EUSO-SPB2 can reach a sensitivity for an energy-squared weighted flux of $\sim 3 \times 10^{-10} \text{ GeV cm}^{-2} \text{ s}^{-1} \text{ sr}^{-1}$, in the energy range $10^7 < E/\text{GeV} < 10^8$. The average cosmic ray flux in this decade of energy is $\sim 3 \times 10^{-7} \text{ GeV cm}^{-2} \text{ s}^{-1} \text{ sr}^{-1}$ [23]. Measurement of the electron and muon component of the shower will be possible via statistical analysis of the full data sample. Such information will be invaluable for understanding the nuclear composition providing an opportunity to clarify the origin of the second-knee. Observation in this energy regime will also contribute to understanding of other subtle features reported in the spectrum.

The simplest interpretation of the ankle is that above $10^{9.6} \text{ GeV}$ a new population emerges which dominates the more steeply falling Galactic population of heavy nuclei. The extragalactic component can be dominated either by protons [13] or heavies [24, 25], with the highest energy particles being subject to photopion production and photodisintegration, respectively. This is the mechanism behind the well-known *Greisen-Zatsepin-Kuz'min* (GZK) cutoff [26, 27]. It has also been advocated that the ankle feature could be well reproduced by a proton-dominated power-law spectrum, where the ankle is formed as a *dip* in the spectrum from the energy loss of protons via Bethe-Heitler pair production [28, 29]. In this case extragalactic protons would already have started to dominate the spectrum somewhat beyond $10^{8.7} \text{ GeV}$. Optical observations of air showers with fluorescence telescopes or non-imaging Cherenkov detectors consistently find a predominantly light composition at around 10^9 GeV [30] and that the contribution of protons to the overall cosmic ray flux is $\gtrsim 50\%$ in this energy range [31–34]. Due to the absence of a large anisotropy in the arrival direction of cosmic rays below the ankle [35, 36], we can conclude that these protons must be of extragalactic origin. At energies above $10^{9.4} \text{ GeV}$, the high-statistics data from the Pierre Auger Observatory suggests a gradual increase of the fraction of heavy nuclei in the cosmic ray flux [31–34]. Within uncertainties, the data from the Telescope Array (TA) are consistent with these findings [37, 38]. In addition, TA has observed a statistically significant excess in cosmic rays with energies above 57 EeV in a region of the sky spanning about 20° , centered on equatorial coordinates (R.A. = 146.7° , Dec. = 43.2°) [39]. This is colloquially referred to as the TA hot spot. The absence of a concentration of nearby sources in this region of the sky corroborates other experimental evidence for heavy nuclei, whereby a few local sources within the GZK sphere can produce the hot spot through deflection in the extragalactic and Galactic magnetic fields.¹

The Galactic to extragalactic transition is likely to extend over a wide range of energies. For protons, the transition is thought to occur in the KASCADE-Grande light ankle at $E \approx 10^8 \text{ GeV}$ [40]. The relative abundance of Galactic nuclei decreases gradually, with nuclei of larger Z decreasing in abundance more slowly than those of lower Z . There are a number of models proposed for this interesting energy range where a transition from Galactic to extragalactic may occur [41–43]. An increase in observations of the varying components in this energy range will help determine the correct model.

¹ Beyond the GZK energy threshold, observable sources must lie within about 100 Mpc, the so called GZK horizon, or GZK sphere.

A plethora of source candidates have been proposed, among the most popular being active galactic nuclei (AGNs), starburst galaxies, and gamma-ray bursts (GRBs) [44, 45]. AGNs are actively-accreting super-massive black holes and are sometimes associated with jets terminating in lobes, which can be detected in radio. The so-called “radiogalaxies” are a sub-class of AGNs, which contain localized regions of intense synchrotron emission known as hot spots. These regions are presumably produced when the bulk kinetic energy of the jets ejected by a central AGN is reconverted into UHECRs [46, 47]. UHECR acceleration is also possible in polar cap regions of the black hole magnetosphere [48, 49]. Centaurus A (Cen A) is the closest radiogalaxy to Earth and has long been suspected to be a potential UHECR accelerator [50, 51]. The Pierre Auger Collaboration has searched for anisotropies in the direction of Cen A scanning the energy threshold between $10^{10.6}$ GeV and $10^{10.9}$ GeV and counting events in angular radii ranging from 1° to 30° [52]. The strongest departure from isotropy (post-trial probability $\sim 1.4\%$) has been observed for $E > 58$ EeV in a window of 15° , see Fig.1; 14 events (out of a total of 155) have been observed in such an angular window while 4.5 are expected on average from isotropic distributions. Starbursts are galaxies undergoing a large-scale star formation episode. Their characteristic signatures are strong infrared emission (originating in the high levels of interstellar extinction), a very strong HII-region-type emission-line spectrum (due to a large number of O and B-type stars), and a considerable radio emission produced by recent supernova remnants. UHECRs could be efficiently accelerated at the terminal shock of a galactic-scale superwind, which is driven by the collective effect of supernovae and massive star winds [53]. Because of the high prevalence of supernovae, starbursts should possess a large density of newly-born pulsars. Due to their important rotational and magnetic energy reservoirs these young neutron stars have been explored as a potential engine for UHECR acceleration [54–56]. A recent study [57] demonstrates that for the most reasonable range of neutron star surface temperatures ($T < 10^7$ K), a large fraction of heavy nuclei survive photo-disintegration losses in the hostile environment sustained by the thermal radiation field from the star. The spectrum of accelerated UHECRs is determined by the evolution of the rotational frequency: As the star spins down, the energy of the cosmic ray particles ejected decreases. As a consequence, the total fluence of UHECRs accelerated in the neutron star magnetosphere is very hard, typically $\propto E^{-1}$ [54]. The arrival directions of the highest energy cosmic rays recorded by the Yakutsk, Fly’s Eye, and AGASA experiments can be traced back to the two nearest starbursts: M82 and NGC 253 [59]. The possible association of the TA hot spot with M82 has not gone unnoticed [60–62], and the possible association of Auger events with NGC 253 and NGC 4945 did not escape attention either [63]. However, as can be seen in Fig. 1, existing data neither favor nor exclude the possibility of starbursts as UHECR emitters. GRBs are short-lived, luminous explosions at cosmological distances, thought to originate from relativistic plasma launched at the deaths of massive stars. The widely accepted interpretation of GRB phenomenology is that the observable effects are due to the dissipation of the kinetic energy of a relativistically expanding fireball [64]. The physical conditions in the dissipation region imply that cosmic rays can be accelerated to energies $\gtrsim 10^{11}$ GeV [65, 66]. UHECR acceleration at GRB internal shocks may also yield a hard source spectrum [67] and consequently accommodate cosmic ray observations [43, 68].

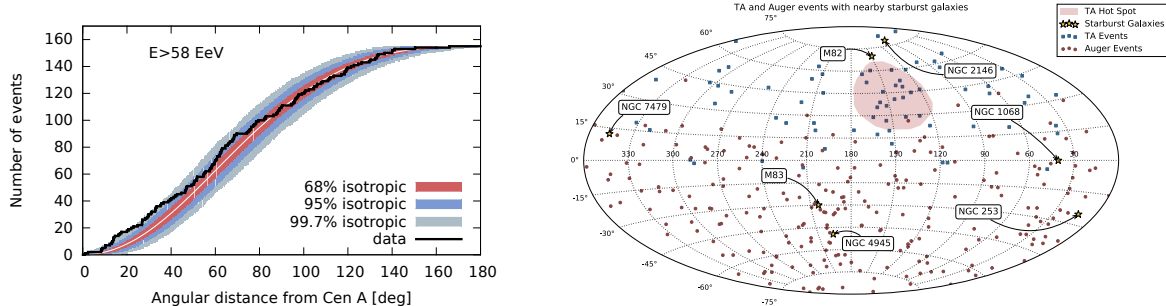


FIG. 1: *Left.* Correlation of Auger events with Cen A. The black line indicates the cumulative number of events as a function of the angular range, for the threshold $E_{\text{th}} = 58 \text{ EeV}$ [52]. *Right.* Comparison of UHECR event locations with nearby starburst galaxies in equatorial coordinates, with R.A. increasing from right to left. The circles indicate the arrival directions of 231 events with $E > 52 \text{ EeV}$ and zenith angle $\theta < 80^\circ$ detected by the Pierre Auger Observatory from 2004 January 1 up to 2014 March 31 [52]. The squares indicate the arrival directions of 72 events with $E > 57 \text{ EeV}$ and $\theta < 55^\circ$ recorded from 2008 May 11 to 2013 May 4 with TA [39]. The stars indicate the location of nearby (distance $< 50 \text{ Mpc}$) starburst galaxies in the *Fermi*-LAT catalog [58], with flux emission (or upper limit) in the gamma ray band $0.1 < E_\gamma/\text{GeV} < 100$ bigger than $5 \times 10^{-9} \text{ cm}^{-2} \text{ s}^{-1}$. The shaded region delimits the TA hot-spot.

Even if cosmic rays include a significant component of heavy nuclei we still expect to observe an anisotropy associated with the heavy component at the highest energies, due to the anisotropic distribution of matter within the GZK sphere [59]. In the event that a correlation with astrophysical sources is present in the data it is important to predefine a search prescription in order to assign a meaningful *a priori* statistical significance to a potential observation. We follow the approach taken by the Auger Collaboration, in which we assume an “interesting” anisotropy result requires a pre-specified chance probability [69]. Given the exploratory nature of the SPB missions we will consider a 1% significance to constitute such an interesting result. For our prescription, we adopt a low energy cutoff of $10^{10.7} \text{ GeV}$, which is in the range where TA observes the hot spot. We chose our candidate objects subject to the following considerations: Even though we do not know the exact declination observable during the flight the majority of candidate objects will be in the southern sky. On the basis of Auger and TA data we assume EUSO-SPB2 will not observe small-scale clustering of events, rather we chose to search for excesses in 20° regions of the sky centered at the source targets. We further assume that UHECRs are accelerated in nearby sources. In particular, we partition the probability budget equally between starbursts and radiogalaxies. More specifically, we consider the nearby radiogalaxy Cen A with a 0.5% budget and starbursts NGC 253, NGC 4945, M83, NGC 1068 (assuming the latter is within the balloon exposure) the remaining 0.5%. If NGC 1068 is not in the field of view we retain the partition of the probability budget equally between starbursts and radiogalaxies. Including GRBs in the prescription would introduce a considerable complexity in the analysis due to their transit nature. Note that this prescription has been designed in time for the launch of the first EUSO-SPB in late

March 2017, implying that we can also use data gathered in this flight in our search.

C. Properties of nearly horizontal air showers developing at high altitude

When the incident cosmic radiation interacts with atomic nuclei of air molecules, it produces fluxes of secondary, tertiary, and subsequent generations of particles. All these particles together create a cascade, called air shower. As the cascade develops longitudinally the particles become less and less energetic since the energy of the incoming cosmic ray is redistributed among more and more participants. The transverse momenta acquired by the secondaries cause the particles to spread laterally as they propagate through the atmospheric target. Most of the air shower particles excite nitrogen molecules in the atmosphere, which fluoresce in the UV. Fast UV cameras aboard EUSO-ESP2 will record the fluorescence light produced by the particle cascades.

If the primary cosmic ray is a baryon, hundreds to thousands of secondary particles are usually produced at the interaction vertex, many of which have energies above the highest accelerator energies [70]. These secondary products are hadrons, mostly pions with a small admixture of kaons and nucleons. When the π^0 's (with a lifetime of $\approx 8.4 \times 10^{-17}$ s) do decay promptly to two photons, they feed the electromagnetic component of the shower. Charged mesons because of a longer lifetime, not only decay but also interact strongly with atmospheric nuclei. The competition between the two processes depends essentially on the balance between interaction mean free path (dependent on the cross-section and the density of the medium transversed) and the mean decay length. Both vary substantially with energy and become equal at a critical energy ξ_c . For a vertical transversal of the atmosphere, such a critical energy is found to be $\xi_c^{\pi^\pm} \sim 115$ GeV for charged pions and $\xi_c^{K^\pm} \sim 850$ GeV, $\xi_c^{K^{0,L}} \sim 210$ GeV, $\xi_c^{K^{0,S}} \sim 30$ TeV for kaons [71]. Hence, below the critical energies the decay probability becomes larger than the interaction probability. Charged pions and kaons give rise to muons and muon-neutrinos in the shower. Neutrinos escape detection carrying roughly 2% of the primary energy, while the highly relativistic muons propagate to the ground.

The number of particles as a function of the amount of atmosphere penetrated by the cascade (X in g/cm^2) is known as the longitudinal profile. A well-defined peak in the longitudinal development, X_{max} , occurs where the number of e^\pm in the electromagnetic shower is at its maximum. X_{max} increases with primary energy, as more cascade generations are required to degrade the secondary particle energies. Evaluating the mean and the dispersion of the X_{max} distribution is a fundamental part of many of the composition analyses done when studying air showers. The generic shower properties can be qualitatively well understood using the superposition principle, which states that a shower initiated by a nucleus with A nucleons and energy E behaves to a good approximation as the superposition of A proton showers with initial energy E/A [72]. This phenomenological assumption relies on the fact that the effect of nuclear binding is negligible compared to the extremely high energies of the incoming cosmic rays. Thus, for a given total energy E , showers initiated by a heavy nucleus have smaller X_{max} than proton induced showers. Shower-muon-richness is also sensitive to the nuclear composition [72].

EUSO-SPB2 will be able to measure for the first time showers which develop nearly horizontally at high altitude, where the density of the atmosphere is low and nearly constant. For such showers, the competition between interaction and decay significantly modifies the average and spread of the X_{\max} distribution compared to the distributions characterizing more vertical showers. This results from the hadrons spending more time in the tenuous atmosphere where they are more likely to decay than interact as compared to a shower developing through an atmosphere of progressively increasing density. At present, hadronic interaction models extrapolated from LHC data can be vetted at higher energies only via air shower observables (like the mean and spread of X_{\max} and muon richness) for showers that impact the Earth [73]. EUSO-SPB2 observations of high-altitude horizontal showers will provide a complementary handle on hadronic interaction models due to the unique environment in which the particle cascades take place.

D. The hunt for astrophysical tau-neutrinos using upgoing air showers

The announcement by the IceCube Collaboration of the observation of 53 astrophysical neutrino candidates in the energy range $10^{4.5} \lesssim E_\nu/\text{GeV} \lesssim 10^{6.3}$ has been greeted with a great deal of justified excitement [74–78]. With these events, a purely atmospheric explanation for the neutrino flux is rejected at more than 5.7σ [78]. IceCube’s discovery represents the “first light” in the nascent field of neutrino astronomy.

A nearly guaranteed neutrino flux originates in the decay of charged pions, which are expected to be produced in pp or $p\gamma$ collisions near the cosmic ray acceleration sites, either in Galactic or extragalactic sources [79–83]. Since cosmic rays and neutrinos may originate at the same sites, searches for correlations in the arrival directions of IceCube events and UHECRs have been carried out [84]. In particular, a possible association between the TA hot spot and IceCube neutrinos has been studied [85]. In pp and $p\gamma$ collisions only muon and electron neutrinos are produced. If we assume the hypothesis of maximal mixing [86], the flavor ratios arriving at Earth should be $\nu_e : \nu_\mu : \nu_\tau \sim 1 : 1 : 1$. Within errors these ratios are consistent with IceCube’s observations [87, 88]. However, the identification of tau neutrinos has remained elusive: no (“double-bang” [89]) events were found in three years of IceCube data, in agreement with the expectation of 0.5 signal events [90].

EUSO-SPB2 will search for up-going air showers produced by tau leptons originating from neutrino interactions below the Earth’s surface [91–93]. If no neutrino candidate is observed, EUSO-SPB2 measurements will help to establish the background for future experiments of this type, like the POEMMA space mission.

There are three types of events which could occasionally be misinterpreted as neutrino induced up-going air showers: (i) random coincidences of excesses of the night Earth background may occasionally exceed the detection threshold of the telescope camera; (ii) signals from high-energy cosmic ray induced showers; (iii) shower-like signals produced by the direct interactions of cosmic rays with the focal plane of the detector.² A

² The night Earth background is a combination of the atmospheric airglow and scattered emission from the

detailed discussion of background events has been presented elsewhere [2].

In summary, the primary objective of using EUSO-SPB2 for neutrino studies is to evaluate in detail the background with which future more ambitious space-based missions will have to contend. An optimist might also hope for detection of a few tau neutrino candidates.

E. Cosmic ray physics using Cherenkov light

It is also possible to exploit Cherenkov light detection to estimate the muon richness of air showers. In an air shower, the electrons, positrons and muons all generate Cherenkov light. In the case of highly inclined showers, however, muons propagate over much larger distances than the electrons and photons, resulting in Cherenkov light topologies exhibiting “halos” or “tails” which are distinct from the spatiotemporal distribution of Cherenkov light emerging from the quickly developing electromagnetic shower component, as discussed in [1]. This can enable searches for photon primaries in an energy regime complementary to other experiments, potentially yielding the best bounds for $10^8 \lesssim E_\gamma/\text{GeV} \lesssim 10^9$, as illustrated in Fig 2. Achieving such an exceptional sensitivity will, of course, require refinement of previously explored techniques to reject the cosmic ray background [1]. Sufficient rejection power is not unprecedented in other cosmic ray experiments; indeed the Auger Collaboration has reported photon bounds at the level of 0.1% of the total cosmic ray flux [97, 98].

The experiment will have sensitivity to the muon component of the air showers, for primary cosmic rays in the energy range $10^7 \lesssim E/\text{GeV} \lesssim 10^{10}$ [1]. This will allow us to test hadronic interaction models beyond colliders energies. The Pierre Auger Collaboration has reported an excess in the number of muons of a few tens of percent over expectations computed using extrapolation of hadronic interaction models tuned to accommodate LHC data [3]. This has been interpreted as a possible signal of new physics at sub-fermi distances [99–102]. The hypothesis of a new physics process is consistent with the non-observation of the muon excess at $E \sim 10^8$ GeV in data collected with the Moscow State University Extensive Air Shower (EAS-MSU) array [103]. However, in this same energy range, $10^8 \lesssim E/\text{GeV} \lesssim 10^9$, a possible excess of muons has been observed with HiRes-MIA [104] and KASCADE-Grande [105]. Therefore, corroborating evidence for the muon excess at lower energies is essential for our understanding of fundamental physics. As discussed in [1] EUSO-SPB2 will have the potential to provide such evidence.

A point worth noting at this juncture is that because EUSO-SPB2 will not observe Cherenkov light in stereo, it will not be feasible to measure all the physical characteristics of the shower simultaneously. With a mono system, we will be sensitive to the number of photons originating from electrons versus muons. However, reconstruction of the primary particle energy for an individual event depends not only on signal size, but also on impact parameter and the depth of the first interaction. In addition, the relation between the number of electrons and muons and the strength of the Cherenkov signal

starlight.

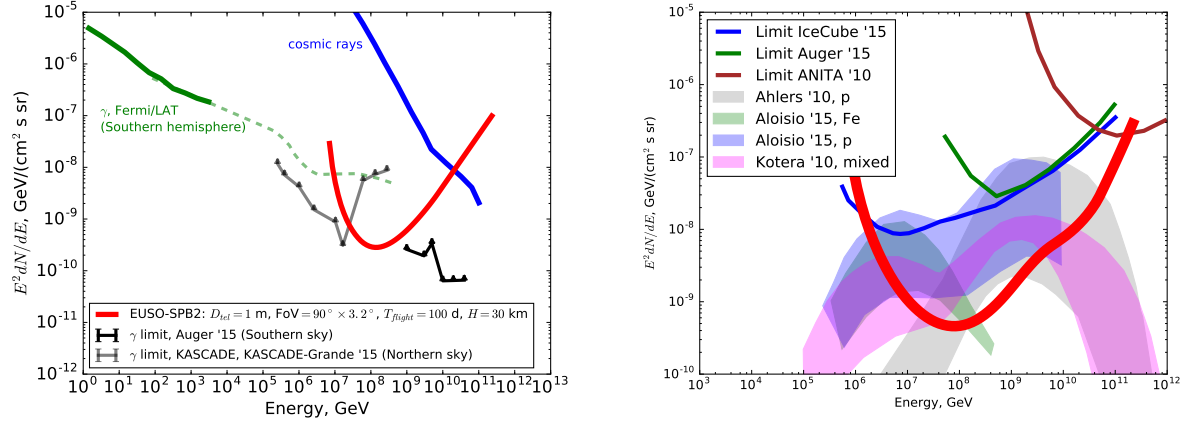


FIG. 2: *Left.* Sensitivity of EUSO-SPB2 to gamma rays. The red line shows the best achievable sensitivity to the photon flux based on the assumption photons can be uniquely identified applying the techniques described in [1]. The green solid line shows the square energy weighted flux of gamma-rays observed by *Fermi*-LAT [94, 95] and the dashed line shows a power-law extrapolation of the square energy weighted spectrum, modified by absorption on cosmic microwave background over the distance scale 8 kpc. The blue curve indicates the cosmic ray intensity [23]. The grey and black lines show current photon limits from KASCADE-Grande [96] and Auger [97, 98], respectively. *Right.* Comparison of the sensitivity of space borne POEMMA to the expected levels of cosmogenic neutrino flux, modelled under different assumptions about UHECR flux composition and radiation backgrounds in the intergalactic medium [108–110]. Limits from IceCube [78], Auger [111] and ANITA [112] are shown for comparison.

in the two components depends on the impact parameter. Therefore, our analysis of the muon content of showers as a function of energy cannot be done on an event-by-event basis, but will require statistical analysis of our event ensemble. We envision using a maximum likelihood approach. We will construct a model for the behavior of the ensemble of measurements that includes free parameters which describe the energy spectrum and the average muon content. The likelihood that this model matches the ensemble of data will be maximized by adjusting these parameters. The result will be a determination of the parameters and the errors of these determinations.

F. NASA's POEMMA

POEMMA will measure orders-of-magnitude more UHECR events than attained by ground-based observatories at $E \gtrsim 10^{10.8} \text{ GeV}$. POEMMA has been designed to reach unprecedented geometrical apertures $> 10^6 \text{ km}^2 \text{ sr yr}$, which, after duty cycle corrections, correspond to annual exposures of more than 10^5 km sr yr at the highest energies. POEMMA will also have high angular resolution (about 1°) and X_{max} determination ($\sim 20 \text{ g/cm}^2$). The unprecedented POEMMA exposure will also provide full coverage of

the Celestial Sphere. This will enable far more sensitive sky maps leading to the discovery of the brightest sources of UHECRs in the sky.

POEMMA will search for astrophysical and cosmogenic neutrinos with two techniques.³ With the same system designed to observe UHECRs based on the OWL design, POEMMA can detect deeply penetrating horizontal showers initiated by all flavors of EeV neutrinos in the atmosphere. In addition, a Cherenkov telescope based on the CHANT concept combined with Cherenkov measurements by the fluorescence telescope can observe the signal produced from tau neutrinos beginning 10^7 GeV (where astrophysical IceCube neutrinos are expected) to 10^{10} GeV (where cosmogenic neutrinos can be discovered, as illustrated in Fig. 2).

POEMMA will also be sensitive to ultrahigh-energy photons. The ultrahigh-energy photon flux is highly model dependent for astrophysical sources, being highly sensitive to the location of the closest sources [113]. Ultrahigh-energy photons are the dominant component of models based on relic decays from the early universe, including super-heavy dark matter [114–120]. A clear detection of these photons would be momentous discovery.

In summary, POEMMA will provide a new window on the Universe and on its most energetic environments and events.

II. TECHNICAL DESIGN OF THE INSTRUMENTS

A. Observation and measurement strategies

Advancements in the study of extensive air showers over the past decades are largely based on larger apertures and exposures to attain more detailed information on the nature and sources of the UHECR flux and its role in the universe. We can now observe these rare particles from balloon altitudes with apertures approaching that envisioned for space-based missions (*cf.* 10% of the original EUSO design envisioned to fly onboard the Internations Space Station (ISS)) and with exposures lasting ~ 100 days with a favorable duty cycle, making NASA's SPB balloon program an excellent opportunity for further advances.

The new SPB platform in Wanaka (45° S, 169° E), New Zealand, is designed to fly at near constant pressure altitude through day-night cycles by maintaining a positive internal pressure, thus enabling Ultra-Long Duration mid-latitude Balloon (ULDB) flights. The edge of the atmosphere provides a distinct vantage point for looking at the developing showers and enhances observations such as the muon generated signals relative to that of the electromagnetic cascade, making possible measurements that can add significantly to the study of the UHECR primary composition.

³ A diffuse flux of neutrinos originates in the energy losses of UHECRs *en route* to Earth. UHECR interactions with the cosmic microwave and infrared backgrounds generate pions and neutrons, which decay to produce neutrinos [106, 107]. The accumulation of these neutrinos over cosmological time is known as the cosmogenic neutrino flux.

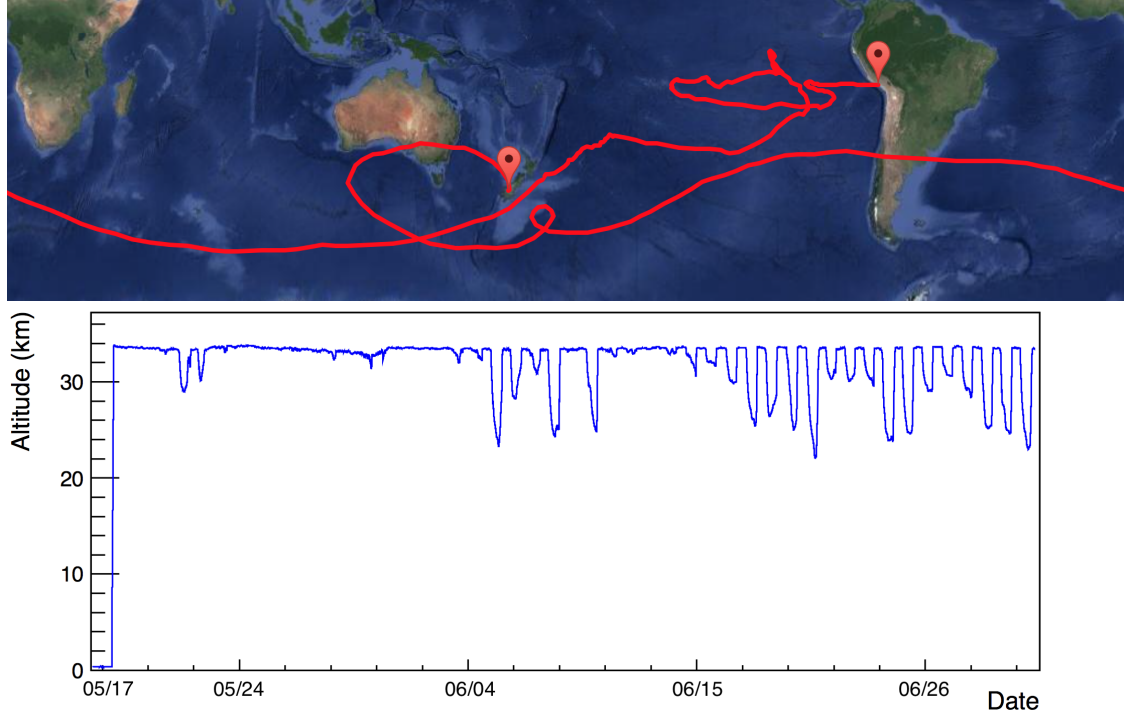


FIG. 3: Flight path and altitude of the first SPB science flight, lifting the Compton Spectrometer and Imager (COSI) [121]. *Top*. Flight path from launch in Wanaka, New Zealand, to termination in Arequipa, Peru. COSI was afloat for 46 days and spent much of its time over the Southern Pacific Ocean. *Bottom*. Altitude profile over the duration of the flight. After the night of June 5th, large altitude drops during the cold nights were seen.

Two balloon flights are proposed: a 1 night CONTinental USa (CONUS) test flight and an ULDB science flight. The test flight in 2020 will be used to verify performance of the instruments and analyze the data collected on background signal levels. The test flight payload will have the same functionality of the ULDB instruments, but the focal surface will be only partially populated to minimize risks that could impact the schedule for a ULDB science flight in 2022. The data acquired during the flight will provide direct knowledge on the anticipated backgrounds during the ULDB mission and allow optimizing the instrument parameters for the mission. It also prepares the team for the challenges of the SPB campaign in New Zealand. The ULDB is well suited to address the science objectives. The mid-latitude flight provides a balance between day/night for powering the instrument and carrying out the night-time observations over a 100 day mission, at an average altitude of 30 km (see Fig. 3).

Three independent telescopes designed for specific measurements provide the data needed to meet the science objectives. A pair of large telescopes will observe the Cherenkov signal from horizontal events and the upward directed Cherenkov signal from air showers produced in the atmosphere. Both telescopes have a field of view (FoV) $3.5^\circ \times 45^\circ$ and they image an annulus centered on the balloon location and a > 100 km

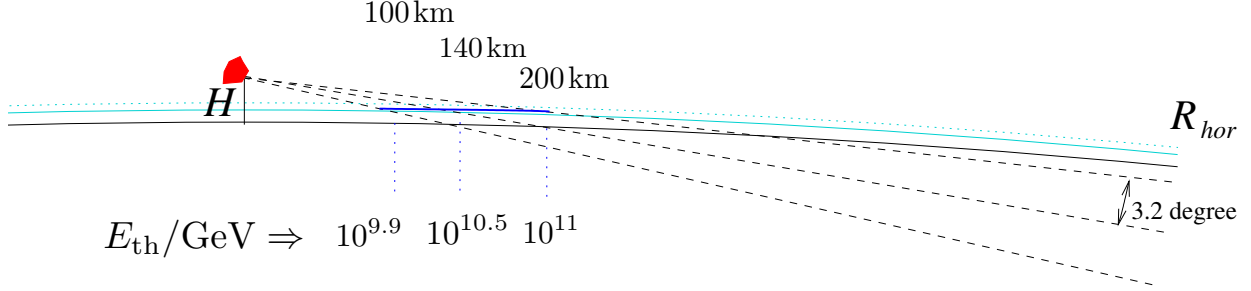


FIG. 4: Schematic illustration of the shower energy and distance detection thresholds.

radius of Earth's surface. Data is acquired at different elevation angles from the horizon to $\sim 10^\circ$ below, see Fig. 4. This amounts to an observational area

$$A_{\text{EUSO-SPB2}} \sim \pi [(200 \text{ km})^2 - (140 \text{ km})^2]/4 = 1.60 \times 10^4 \text{ km}^2, \quad (1)$$

which is about 10% of the area it would have been observed by EUSO onboard the ISS:

$$A_{\text{EUSO}} \sim \pi [400 \text{ km} \tan(\pi/6)]^2 = 1.67 \times 10^5 \text{ km}^2, \quad (2)$$

where the factor of 1/4 in (1) accounts for the fact that EUSO-SPB2 will observe $\sim 90^\circ$ of a full circle and where in (2) we have taken the nominal EUSO FoV of 60° and a circular orbit for ISS at an altitude of 400 km [122]. A third telescope with a smaller FoV $3.2^\circ \times 28.8^\circ$ will measure the intensity of the slower fluorescence signals produced by extensive air showers, imaging the event trajectory as the cascade develops down through the atmosphere. The fluorescence sensor will be configured using the components recovered from EUSO-SPB.

No imaging is required for the upward Cherenkov flashes that are focused to a small spot on the focal plane at the position of the event within the FoV. The signal amplitude corresponds to the number of photons collected by the telescope, which depends on impact parameter and energy. A fast coincidence between multiple detectors is needed to suppress false triggers from the charged particle background. These upward Cherenkov flashes arrive at the balloon platform with pulse durations of ~ 10 ns and essentially parallel. The telescope's FoV insures the primary particle trajectory passed through Earth.

The Cherenkov and fluorescence signal have greatly differing signal characteristics and therefore require separate focal sensors. For fluorescence measurements, the angle of the telescope defines the nearest distance within the FoV that in turn determines the observable energy threshold for showers; see Fig. 4. The atmospheric cascade can be imaged as they propagate down through the atmosphere producing a video clip of the air shower evolution at $2.5 \mu\text{s}$ frame rate; see Fig. 5. Similar measurements will be made by the EUSO-SPB flight this year looking at the nadir. The EUSO-SPB2 mission would increase the event rate by a factor of 5 as a result of the balloon-payload design and observation strategy. The time evolution of the fluorescence signals extends over 10's to

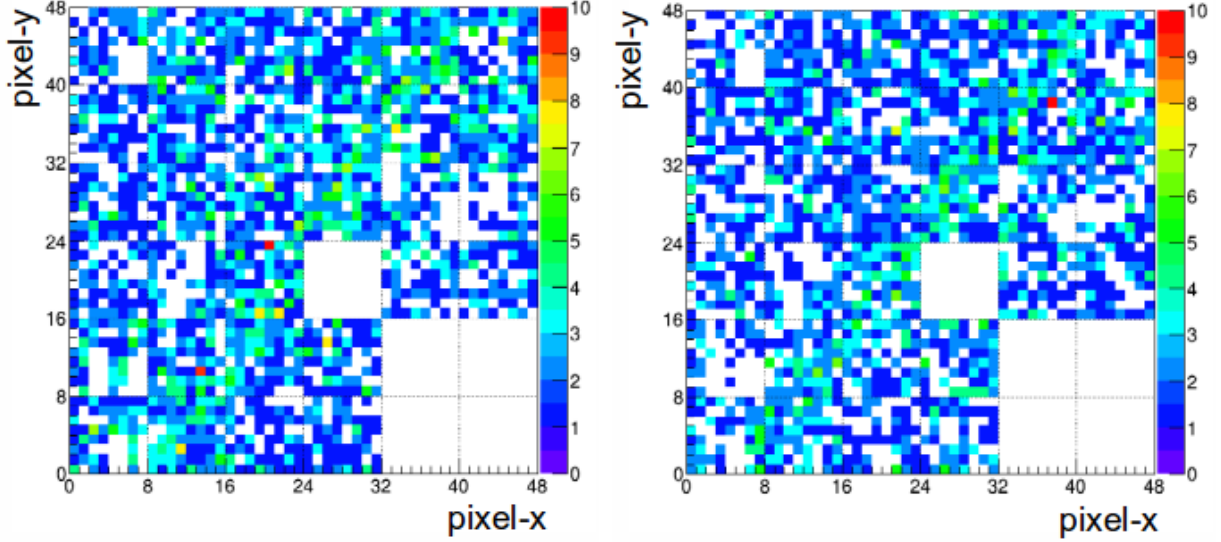


FIG. 5: Comparison of a shower measured by the EUSO-TA pathfinder on May 13, 2015 (left) and a shower simulated by CONEX [123] (using the energy, zenith angle, and impact parameters measured by BRM-TA Collaboration for that event) and processed by the *Offline* software (right). The color-scale indicates the number of counts integrated over all the gate time units ($2.5 \mu\text{s}$ time bins) during which the shower was crossing the EUSO-TA FoV.

100's microseconds. Spatial and temporal data are used to determine the direction and energy of the primary particle.

The observable Cherenkov signals generated from nearly horizontal showers differ greatly from lower inclination events. The charge particle distributions generated from nearly horizontal showers observed at large distances ($\sim 300 \text{ km}$) are shown in Fig. 6 and the longitudinal Cherenkov emissions for gamma-ray, proton, and iron primaries are also compared in Fig. 6. In the region of shower maximum electron emissions are dominant producing fluorescence and Cherenkov photons, but beyond this region the long lived muon component is seen to exceed the Cherenkov emission rates of electrons. We exploit this feature of the muon Cherenkov signal at large distances from the shower, together with the small Cherenkov angle ($< 1^\circ$ to 1.5°) to discriminate the primary particle identity from the image formed on the focal plane. Simulations of the image formed by the Cherenkov signal from showers generated by protons, photons, and iron primaries are shown in Fig. 7. In these images, the muon component (or lack of) is responsible for the details in each image. The gross properties of the photons reaching the telescope are within the Cherenkov cone angle $\sim 1^\circ$ and form an image on the focal plane at the azimuth angle of the event, which varies little event to event due to the short vertical projections of a few degrees. However, the detail structure within the image of the event, as recorded on a focal plane, depends on the impact parameter (distance of closest approach) that can produce a "halo" or "tail" feature within the image. The arrival time of the photons creating this image depends on the distance away they were generated. Since the muon

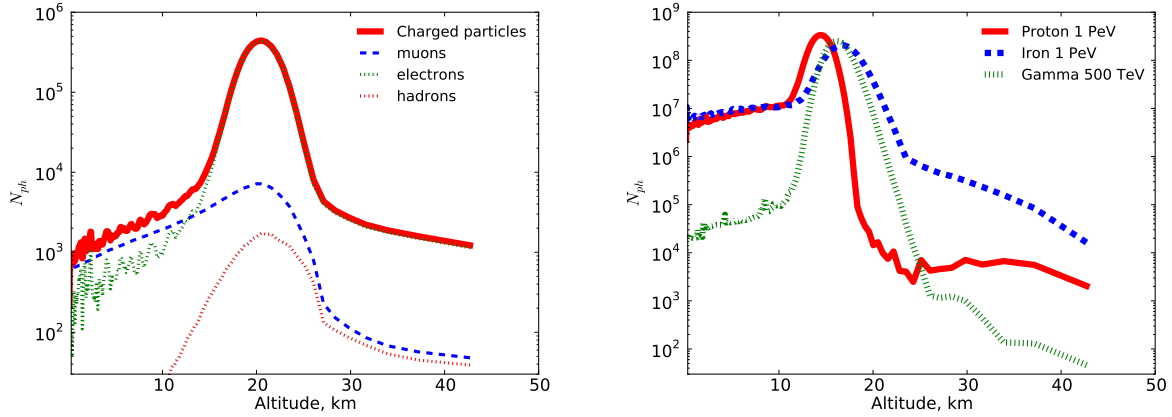


FIG. 6: *Left.* Longitudinal profiles of charged particle distribution in an air shower initiated by a 1 PeV energy proton incident at a zenith angle $\theta = 87^\circ$. *Right.* Longitudinal profiles of Cherenkov light emission of an air shower initiated by a proton (red solid line), an iron nucleus (blue dashed line), and a gamma-ray (green dotted line), with $\theta = 87^\circ$ [1].

speed exceeds that of the Cherenkov photons, photons produced early in the event arrive the latest and visa-versa.

B. Integrated gondola

1. Overview

The gondola provides mounting for the telescopes, instrument subsystems, and balloon equipment for the mission. It is suspended from a pointing rotator used to maintain illumination of the solar array panel during daytime and to point the instruments favorably during nighttime operations. The solar array panel serves as a sunshade for the instrument deck. The telescope focal surfaces are further protected from accidental exposure to direct sunlight by tilting the telescope to the stowed position which acts as a full-aperture stop. The electronics boxes are consolidated in the interior of the deck plate and in close proximity for ease of cable routing. A schematic view of the gondola is shown in Fig. 8. The mechanical design will be refined to meet load limits, volume constraints and safety requirements levied by NASA, the launch vehicle and range operations.

2. Pointing control

The gondola requires modest pointing control to maintain stability for the required observations. Analysis of data from past flights shows that the stability in the elevation angle will be within $\pm 0.1^\circ$ over the course of a night, see Fig. 9. Low frequency variations will not impact light collection during observations as the amplitude is $< 5\%$ of the

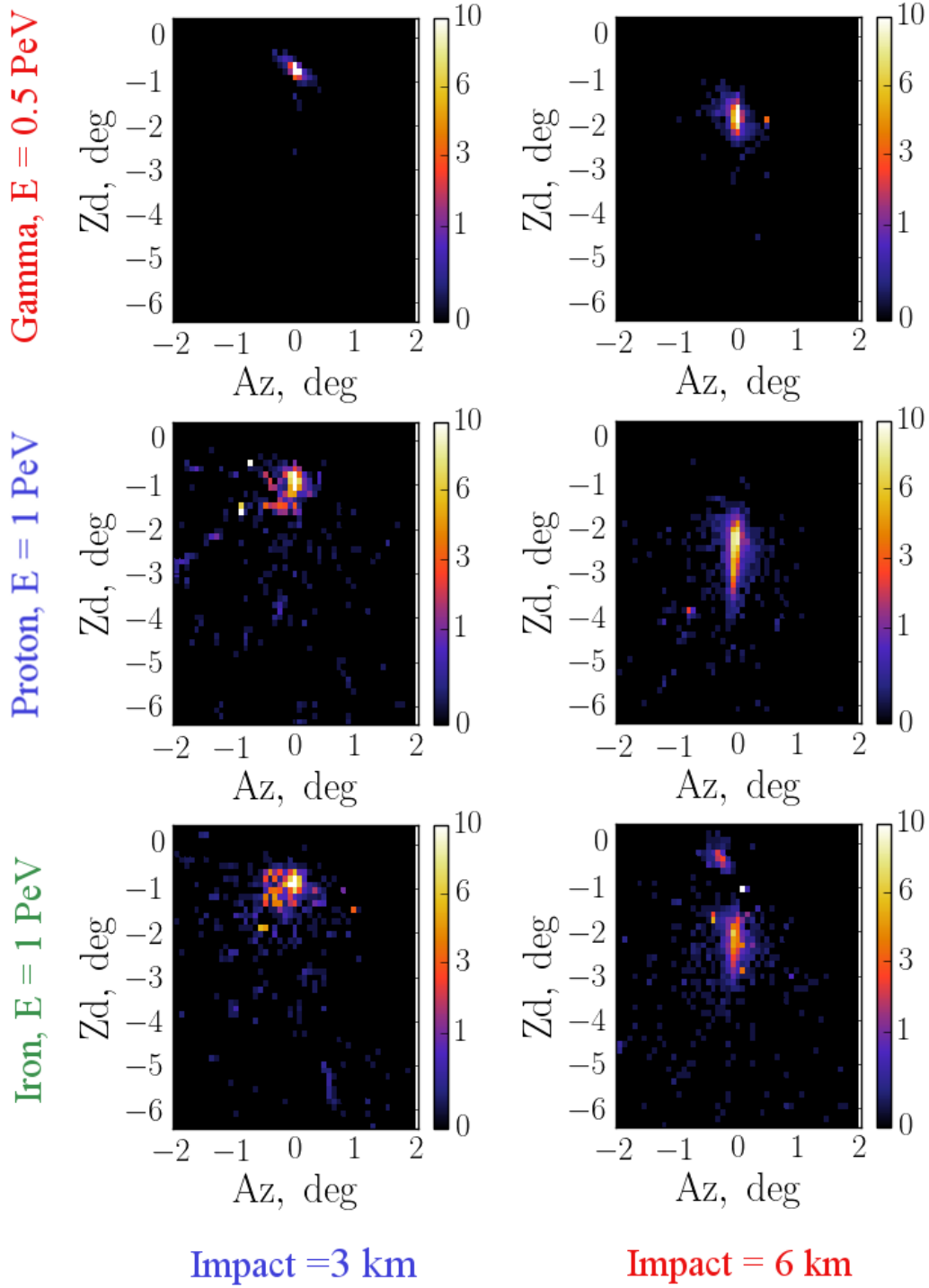


FIG. 7: Images and time profiles of 0.5 PeV gamma-ray, 1 PeV proton and 1 PeV iron induced air showers with $\theta = 87^\circ$. The left column shows the images for showers with impact parameter $d = 3$ km, and the right panels are for $d = 6$ km [1].

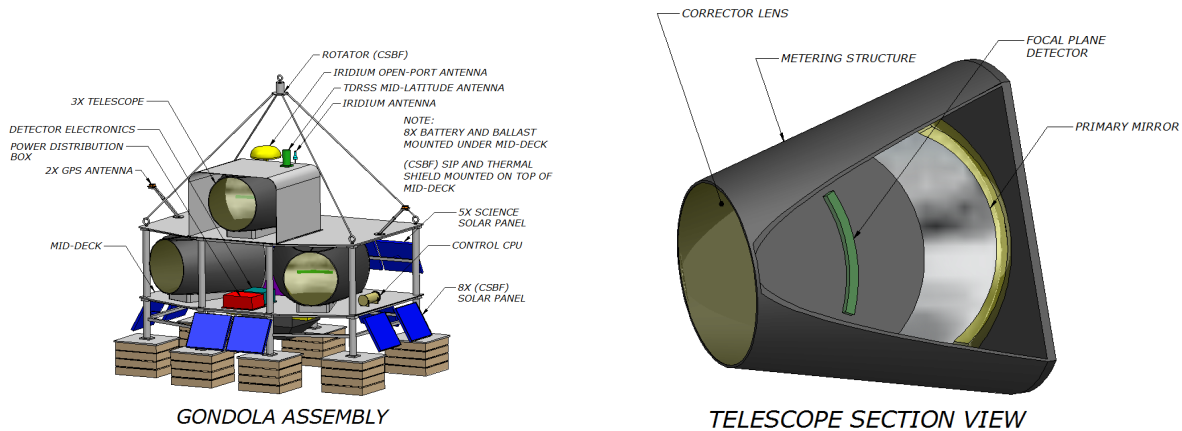


FIG. 8: Concepts of the integrated balloon gondola (left) and one telescope assembly (right).

full FoV. Any offset of the gondola due to mass distribution or cable tension will be compensated by tilting the telescope and monitoring them through inclinometers. A single ballast hopper will be used and centered below the gondola to avoid inducing torques when ballast releases are made to control the balloon flight path.

Horizontal (azimuth) control of the FoV is used to optimize exposures by steering toward regions with reduced clouds and scenes with lower levels of moonlight. The preferred method for night time pointing control makes use of the Columbia Scientific Balloon Facility (CSBF) rotator, but using Global Positioning System (GPS) as feedback instead of the sun-sensor. This can be commanded from the ground but will include the onboard computer in the loop to insure reliable communication with the rotator control equipment. The onboard computer will also use the GPS system for data on pointing knowledge that will be downloaded as part of the telemetry stream for analysis. The resolution in pointing knowledge exceeds stability requirements.

Adjustments to the telescope FoV will follow the science observation plan developed for the mission. The plan calls for extended exposures lasting several hours and potentially all night minimizing variations seen in Fig. 9. Default pointing directions will be loaded on the computer prior to launch and these values are updated throughout the mission. The operations team will monitor satellite based images to determine preferred viewing directions throughout the mission. Typical observations will seldom have multiple adjustments during a night.

3. Power system

The instrument will be powered from batteries at night that are recharged each day using solar panels. A single solar panel will be used as it will be pointed at the sun by the rotator. From our EUSO-SPB experience, we have found that the optimum solar panel tilt for flights from Wanaka, NZ is 15° from vertical.

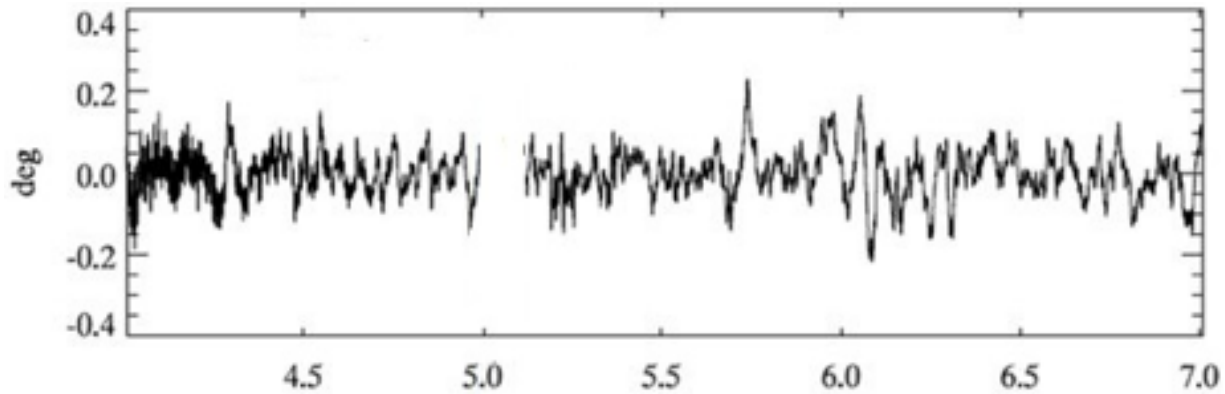


FIG. 9: Measured pitch angle of a passive gondola at float altitude over a 3 hour period.

The solar power system will be designed based on experience gained with EUSO-SPB. We propose to use custom-made 27" \times 31" solar panels with a 6 by 5 configuration of SunPower cells including bypass diodes. The solar cells will be encapsulated within EVA based laminates and subsequently mounted to custom aluminum core, FRP faced honeycomb sandwich substrates to form each panel. Each panel will produce 100 watts at float. We will employ six panels wired in two series strings of three panels each to provide the voltage needed to charge a 24 volt battery pack.

For the battery pack, we propose to use lithium-Ion batteries from Valence U1-12XP. These 40 Ah batteries weigh 13 kg and have been flight-proven by CSBF. 20 of these batteries will provide 400 amp-hours, enough capacity to provide 600 watts of nighttime power for up to 16 hours of darkness. The battery pack will consist of 10 strings, each with two batteries in series.

The batteries will be charged during the day using Morning Star S-MPPT-30 charging controller. This system will operate the solar panel at its peak power point to harvest the maximum power from the panel while charging the battery pack.

4. Telemetry

Primary command and telemetry will be through the Iridium Pilot or Certus system which can support non-continuous data rates of 100 kbps (Pilot) to 1.4 Mbps (Certus). On-board storage will be used to buffer data between downlink opportunities. An independent secondary command and telemetry path will use the Iridium Short-Burst Data system for continuous limited bandwidth (255 bytes/minute) command and state monitoring. During the CONUS engineering flight a continuous 740 kbps line-of-sight transmitter will be flown which will allow extensive science and engineering data to be collected for analysis of system performance.

C. Optics design

Previous EUSO optics pursued wide fields of view (WFOV) by employing purely refractive designs. For this new balloon observatory, the WFOV is only in one direction; namely, along the horizon. The vertical field of view (FoV) is only 3.2° . A well-known design form for achieving good image quality over a wide field is the Schmidt telescope: a catadioptric design, consisting of both reflective and refractive optical elements. The Schmidt design utilizes a spherical primary mirror with the stop at its center of curvature which eliminates coma and astigmatism, and a refractive plate placed at the stop which corrects the spherical aberration. The impact of field curvature is eliminated by curving the array of detectors.

In Fig. 10, we show a spherical mirror which focuses collimated light emanating from the left. The red (green) rays show how light from an object point on-axis (off-axis) will intersect the mirror and define the location and size of the stop, and therefore the entrance pupil for the system. Off-axis rays, top and bottom, intersect the mirror at far different angles of incidence, unlike the rays for the on-axis beam. The off-axis light will suffer from coma and astigmatism in addition to the spherical aberration found in both beams. However, as shown in Fig. 10, by placing the stop at the center of curvature of the spherical mirror, the off-axis rays intersect the mirror in the exact same manner as the on-axis beam. Thus, stop position eliminates the coma and astigmatism, but the image still suffers from spherical aberration. Spherical aberration is a rotationally symmetric deviation from perfect focusing wavefront that follows a 4th, 6th, and higher even-powered radial polynomial form, where the higher orders appear as the aperture diameter increases.

To eliminate the spherical aberration, a refractive plate is placed at the stop which provides the opposite wavefront deviation generated by the spherical mirror. Since the deviation, at the lowest order, follows a ρ^4 form, one surface of the plate will have this form. However, for broad spectrum applications, the addition of this refracting component creates a wavelength dependent aberration. Though the mirror creates the same geometrical error for all wavelengths, the refractive corrector will only perfectly correct the error for one wavelength. To reduce the image degradation from spherochromatism, a very small amount of optical power, ρ^2 , is typically added to the corrector surface which balances some of the residual chromatic power and spherochromatism.

The optic specifications are derived from the science requirements and sensor resolution. For both the Cherenkov and fluorescence imaging systems, the sensors have position resolution of 3 mm, and requiring angular resolution of 0.2° degrees. The required aperture area has been computed to be 0.61 m^2 , which includes obscuration by the sensors. The full FoV is $45^\circ \times 3.2^\circ$ for the two Cherenkov telescopes and $28.8^\circ \times 3.2^\circ$ for the fluorescence telescope system. These specifications lead to an equivalent focal length (EFL) for the fluorescence imager of 0.83 m, and for the larger Cherenkov imager, an entrance pupil diameter of 0.967 m, meaning that the optic is operating at F/0.86.

A baseline design was completed using Zemax [124], with the specifications listed in Table I and shown in Fig. 11. The material selected for the corrector is an UV transmitting poly methyl methacrylate (PMMA) well known to the EUSO team and successfully used

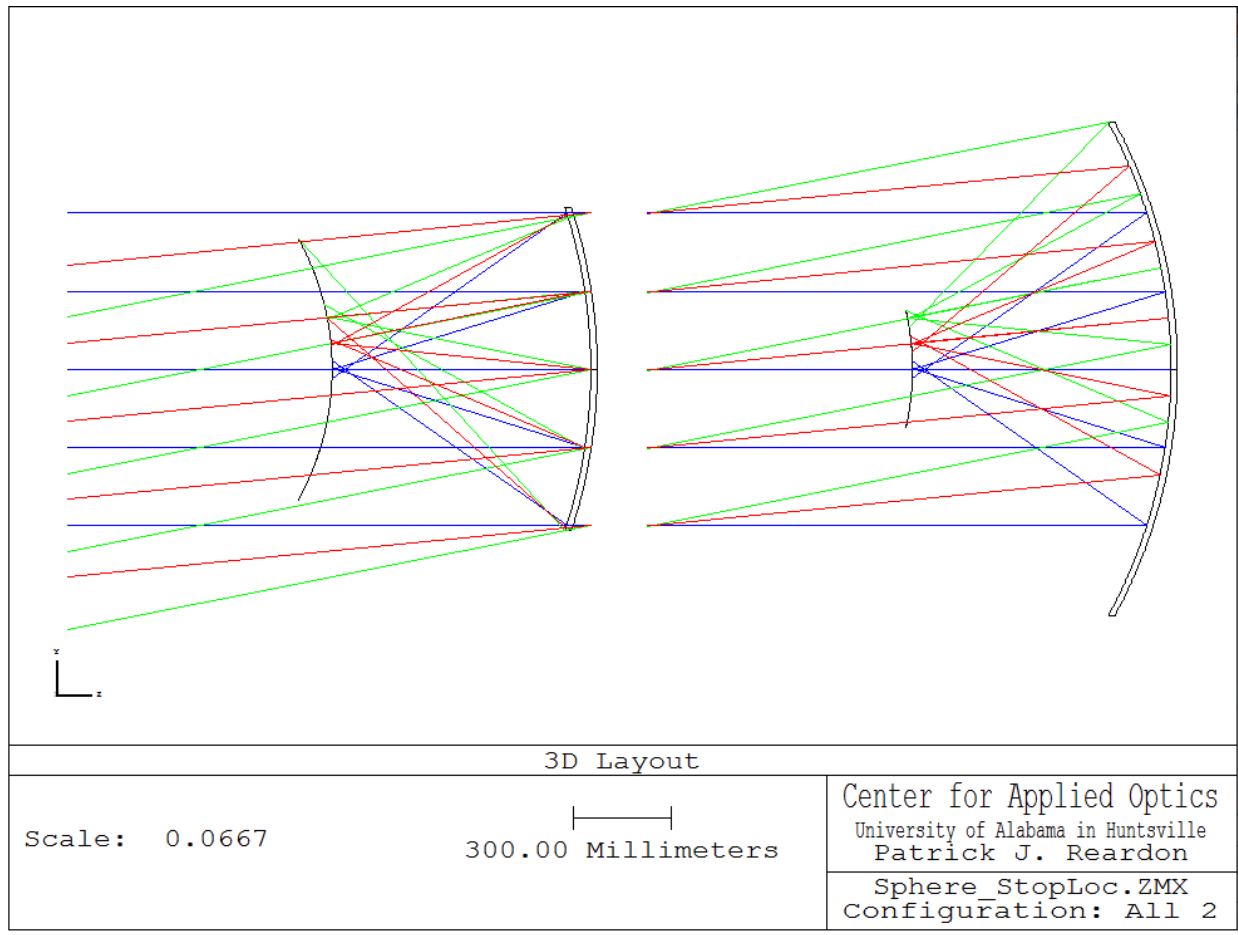


FIG. 10: Imaging of a distant object with a spherical mirror with the stop at the mirror (left) and the stop at the center of curvature of the same mirror (right). Placing the stop at the center of curvature eliminates coma and astigmatism purely by symmetry, but the cost is a larger diameter mirror.

in several prototype systems. To achieve sufficient image quality, the design optimization varied: (i) the radius of the primary mirror; (ii) the spacing between the primary mirror and the corrector; (iii) the location of the physical stop, (iv) the shape of both corrector surfaces including the spherical radius and even powered radial deformations out to the 6th order term; and (v) defocus. This design study concluded successfully easily meeting the clear aperture and the 3 mm spot size for both applications. The expected performance is shown in Figs. 12 and 13. Given the successful baseline performance, the innovative approach for acquiring interlaced horizontal and vertical detection required a modified optical solution. The desire is to create two horizontally separated spots, separated by 25 mm (1 multi-anode photo-multiplier (MAPMT) width). This “bi-focal” solution is to split the spherical mirror along a horizontal line and rotate the top and bottom halves about the vertical axis. The amount of rotation of the two spherical sections is $\pm 0.4^\circ$, yielding a relative angular difference of $\pm 0.8^\circ$.

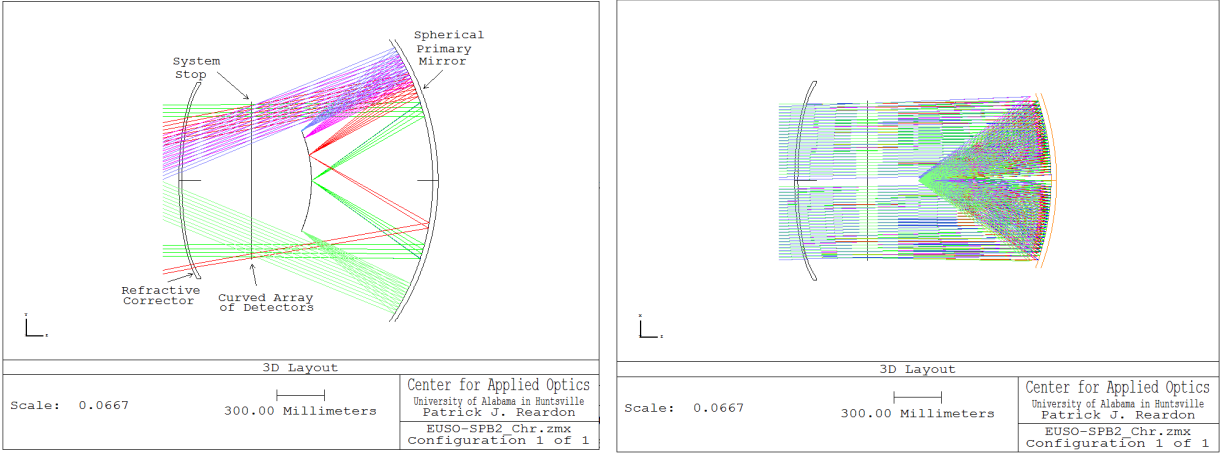


FIG. 11: *Left.* Wide-field cross section showing, from left to right, corrector, physical stop, curved image and spherical primary mirror. Obscured rays are blocked by detector 2. *Right.* Narrow-field cross section showing, left to right, corrector, physical stop, curved image and spherical primary mirror. Obscured rays are blocked by detectors.

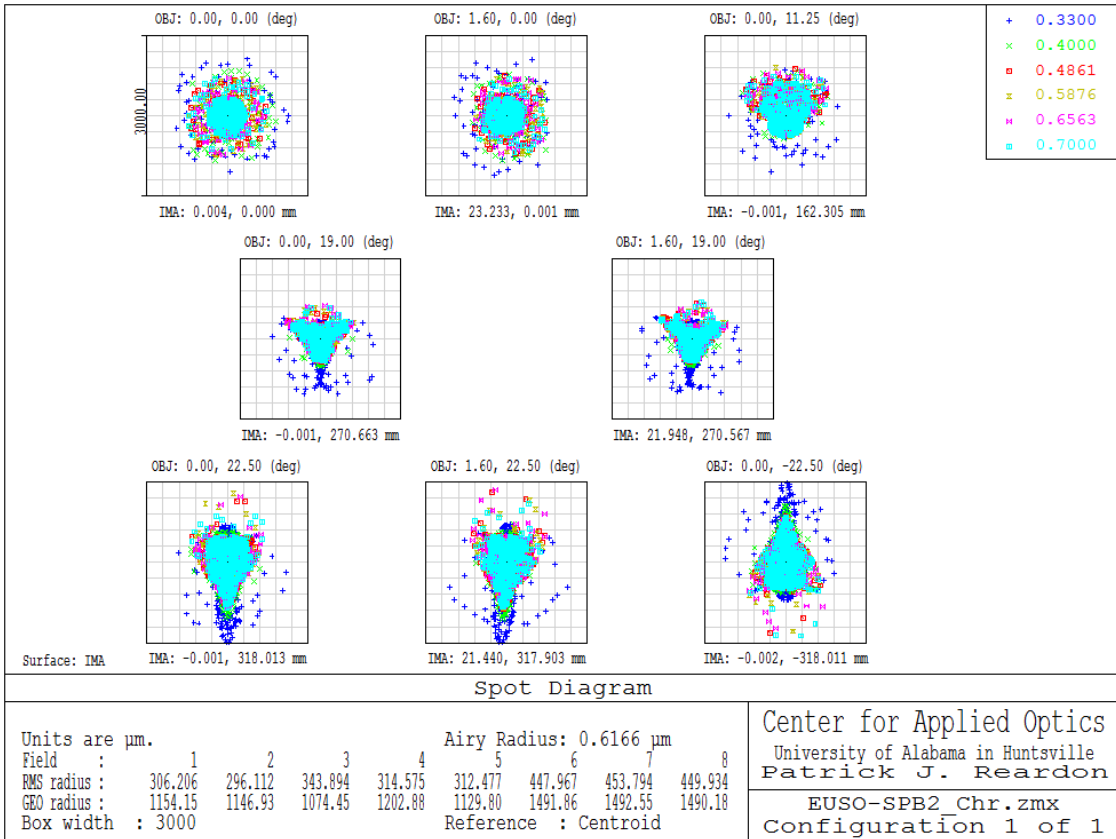


FIG. 12: Spot diagrams across one half the horizontal field, all fitting in the 3 mm^2 detectors.

TABLE I: Specifications of the design.

Element	Material	Shape	Dimensions
Corrector	UV Transmitting PMMA	Sphere $+AR^2 + BR^4$	Thickness = 20 mm Diameter = 1260 mm
Stop		Flat with hole	441 mm from corrector
Primary	CFRP	Spherical, concave $R = -1604$ mm	1.8 m \times 1.1 m 1602 mm from corrector
Image surface		Spherical, convex $R = 830.6$ mm	828 mm from corrector

Surface	$R(\text{mm})$	A	B
1	781.648	-4.17888×10^{-4}	-2.15028×10^{-10}
2	738.415	-4.92112×10^{-4}	-1.75838×10^{-10}

A preliminary tolerance analysis has been performed that indicates this system is extremely insensitive to misalignments. For each parameter, doubling the spot size requires: (i) lateral decenters of the corrector by more than 11 mm vertically or 7 mm horizontally; (ii) tilts of the corrector exceeding 6° ; (iii) mirror slope errors must exceed 1 arc minute (a 0.010 mm amplitude error with a period of 63 mm); (iv) corrector surface slope errors exceeding 4 arc minutes of slope; (v) radius error on the spherical mirror must exceed 20 mm; and finally (vi) refractive index errors, either isotropic, or spatially varying, must exceed any reasonably expected deviations to yield a measurable performance error.

Thermal soaks and gradients can impact the form of the optical elements, the refractive index of the corrector and the positions of the elements due to impacts on the structure. Misalignments tend to have minimal impact on the image quality, but large misalignments in flight could shift the apparent position of the detector array which could either result in a pointing uncertainty or an aberration if the motion results in significant defocus. These optic considerations will be included in the thermal analysis of the gondola.

D. Focal plane detectors

1. Muon Cherenkov sensor

The baseline focal surface detector uses a segmented linear architecture to identify the primary particle from its shower characteristics. This architecture fits within the scope of the project. A technology development effort aimed at improving on the focal plane architecture and demonstrating it is also included to meet future measurements needs, including potentially additional flights of the EUSO-SPB2 instrument.

The focal plane detector is built up from sensor strings based on MAPMTs followed by custom front-end electronics to condition the signals and interface to a commercially available off-the-shelf (COTS) fast analog-to-digital converter (ADC); e.g. AD9637. These

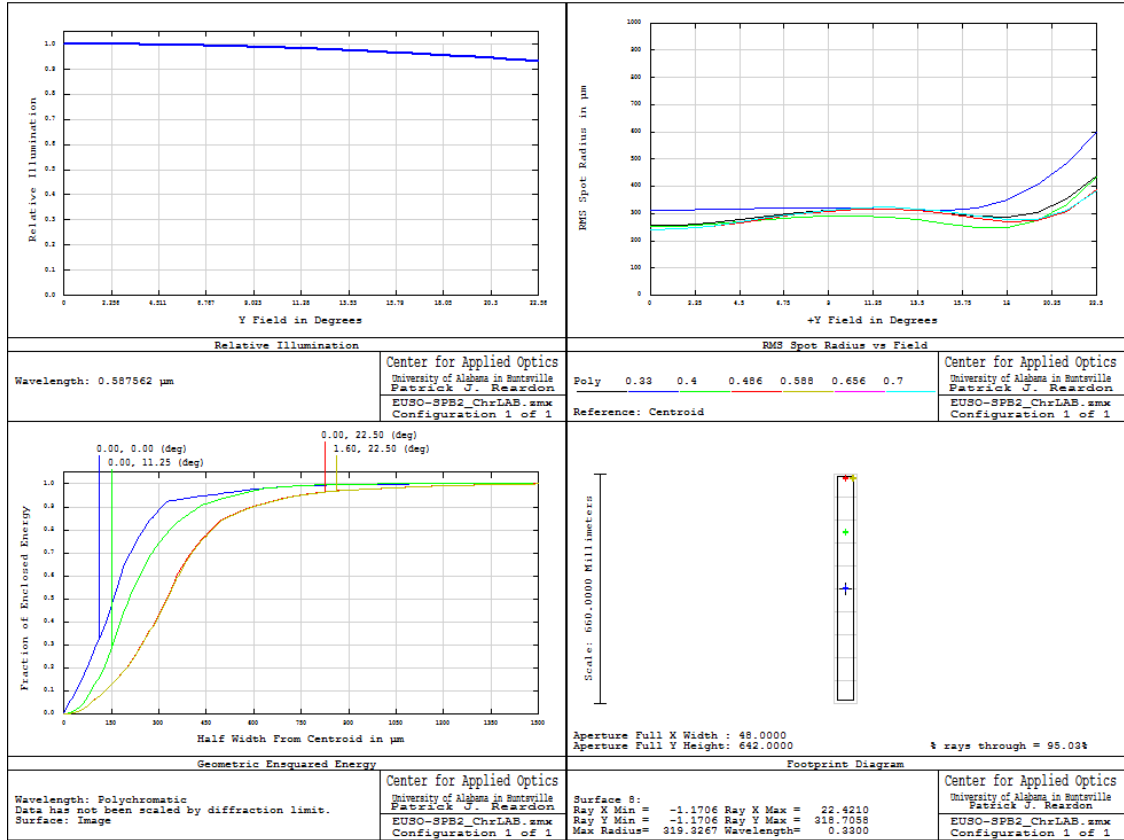


FIG. 13: *Up-left.* Relative throughput only shows minor cosine falloff over full 54° FoV. *Up-right.* RMS spot radius as a function of FoV. *Down-left.* The ensquared energy shows that nearly all the energy fits inside squares of 1.8 mm width. *Down-right.* Location of analyzed spots on the detector array.

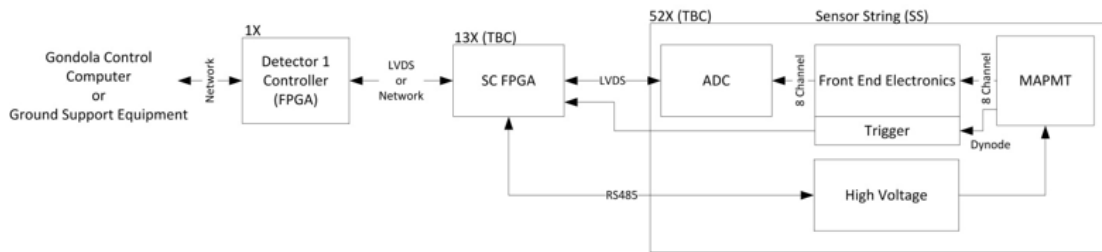


FIG. 14: Basic element of focal plane detector for imaging the Cherenkov signals.

components are controlled through firmware in a field-programmable gate array (FPGA) that interfaces between the sensor string and the data system. In Fig. 14 we show a block diagram of the concept. It will be replicated, as shown, to fill the full area of the focal surface. We will consider a further development of the readout system to adapt the technique conventionally used in Cherenkov telescopes (such as the DigiCam [125]),

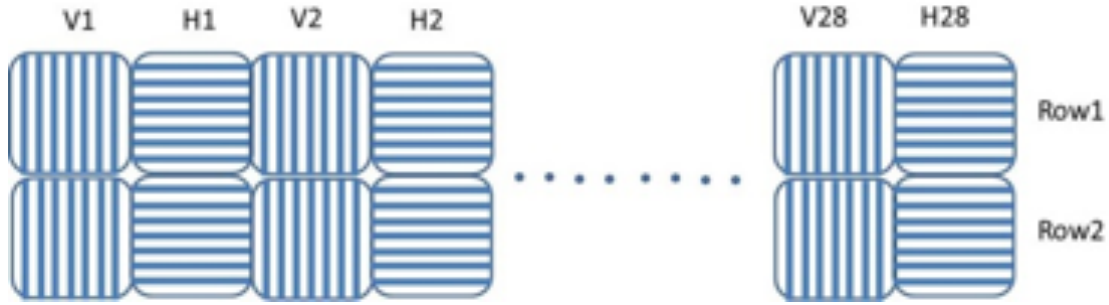


FIG. 15: MAPMT arrangement concept to measure profiles of the image in the vertical and horizontal directions.

which would make possible reading out at the pixel, rather than the strip level. The upper half of the focal plane uses MAPMTs with the anodes aligned along the horizon and the MAPMTs in the lower half of the focal plane are aligned perpendicular to the horizon. The two images produced by the binocular mirror will fall on these two halves of the focal plane to enable location of the image with single pixel resolution, see Fig. 15.

An optical filter will be used to limit the bandwidth of the arriving photons. When convolved with the photo-cathode response, the combination will provide the strongest detectable signal from muons relative to background. We have chosen the Schott VG9 filter which peaks at 525 nm, with 70% transmission and excludes wavelengths below 400 nm. This together with Hamamatsu's extend green photocathode improves the response in the intended band and limits the long wavelength response below 675 nm.

These filters are glued to Hamamatsu R11265-64 photomultipliers (PMTs), which have been designed for close-pack applications like EUSO. These 64-anode MAPMTs provide a 78% fill factor on the focal surface. We bond the 8 pixels in each row together making a linear device with 8 anodes per PMT. The dimensions of each row are $3 \times 23 \text{ mm}^2$. Each MAPMT is mounted on a PCboard that includes an high voltage (HV) supply (C10940-03-R2) and front-end electronics (FEE). The PMTs are mounted in a curved fixture to match the optic design and provide attachment points for mounting at the focal surface.

Each channel's signal is conditioned by the FEE and relayed to the ADC that continuously samples the PMT output. Digitized values are processed in a pipeline with a depth of 16 samples. The ADC has selectable speeds from 10 to 80 Msps. Our studies show that 10 Msps will provide the required timing information and fit within the limit of the pipeline depth. The FPGA will monitor each MAPMT and trigger on the signal. This trigger will initiate a download of the data from the pipeline. The data will then be transmitted to the onboard computer. Following the readout, the sensor string will be re-enabled to continue operations. Periodically the FPGA also stores data from each of the sensors strings to record the unbiased background signals from the telescope.

Image processing is required to recover the event from the two recorded linear profiles. This processing is done on the ground in data analysis, which uses the linear data acquired together with the timing information, measured background signals, and simulations of shower signals (triggered by photon, protons, and iron primaries). The data are sufficient

for event identification for events with large impact parameters, as illustrated in the right column of Fig. 7. The “halo” signal for events with small impact parameters are readily measured using the linear anodes orientated normal to the horizon, as shown in the left column of Fig. 7. The data from both images will be analyzed using imaging reconstruction techniques to improve the sensitivity to the primary composition.

The time profile of the Cherenkov signal contains information on the development that supplements the analysis of the linear data. The arrival time of Cherenkov photons depends on where along the shower track they were generated, with the earliest arriving photons originating from the point on the shower nearest to the detector. The arrival time of the signals indicated from where along the shower they originated. This provides leverage for identification of the muon content and thus the identity of the primary particle. The sharpness in time of the strong (electron) shower signal is influenced by the interaction processes. As discussed above, the absence of knowledge of the shower impact parameter makes it necessary to use ensemble analysis techniques to extract information of the primary particles.

2. *Upward directed Cherenkov signals*

The focal surface detector for the upward directed Cherenkov signals is based on the sensor string described in the preceding section. Since no image information is required, the dynodes are used to form a trigger between paired MAPMTs to reduce false triggers from charged particle interactions in a single PMT. The filter is selected to accommodate more signal bandwidth (300 nm to 550 nm from ground base Cherenkov telescope range). The ADC for each triggered PMT records the intensity of the signals for analysis of the Cherenkov pulse.

3. *Fluorescence sensor*

The fluorescence detector of EUSO-SPB2 will built on the experience of EUSO-SPB. The 2017 flight will carry a full photon detection module (PDM) with 2304 pixels and an optical system for a square FoV $12^\circ \times 12^\circ$. The EUSO-SPB PDM is self-triggering. It captures video clips of the slow (10-100 microseconds) fluorescence signal from UHECR events. The lens system is not expected to survive termination and recovery. It will be replaced by mirror with higher optical through put and tighter focusing that will sharpen the contrast of tracks signals to background by a factor of 2. This in turn increase the sensitivity of the instrument to horizontal extensive air showers viewed with the detector pointed near the horizon. To match the new FoV now looking at the horizon requires repackaging of the PDM. The PDM is built from 9 elementary cells (EC), each of which is a self-contained detector comprised of 4 MAPMTs, HV, FEE and trigger electronics that can be connected in parallel. In order to cover a larger observation area we will change the EC layout for the PDM from 3×3 to 1×9 configuration. Additional options will be considered based, in part, on the performance of the PDM during the 2017 EUSO-SPB flight.

4. *Infrared camera*

EUSO-SPB2 will have a set of infrared cameras to monitor the cloud coverage in the field of view of the Cherenkov and fluorescence detectors. The design will be an update of the University of Chicago Infrared Camera (UCIRC) built for monitoring cloud coverage during the EUSO-SPB flight. UCIRC uses two infrared cameras with different wavelength filters (10 micron and 12 micron) to capture images of cloud cover in EUSO-SPB FoV. The two infrared images taken every minute determine the temperature (and therefore the height) of clouds between EUSO-SPB and the ground. The design, construction, and testing of UCIRC2 for EUSO-SPB2 will be done at Chicago with similar image reconstruction and pixel-by-pixel temperature calibration procedures done for UCIRC.

5. *Testing plans*

Testing is done at the component and subsystem level to confirm performance and workmanship quality. It is continued as we integrate to higher levels. System level testing of the telescopes will include ground-based and high altitude tests to evaluate overall performance of the instrument. The EUSO-SPB instrument was co-located at the TA in Utah and tested using fluorescence signals from extensive air showers and a calibrated laser to permit studies of the trigger levels, trajectory reconstruction and signal resolution. The EUSO-SPB2 telescopes will be tested using a similar approach for Cherenkov signals in addition to fluorescence. The CONUS balloon flight will provide essential data for further tuning of the instrument parameters before the science flight.

6. *Advanced sensor development*

An advanced sensor will be developed to take full advantage of the information contained within the images of the Cherenkov signal in discriminating primary particle identification. The imaging system currently (SPACIROC3) being developed by the EUSO Collaboration is intended for fluorescence measurements. It uses a cadence time of $2.5 \mu\text{s}$ to measure the slow fluorescence signal. An application-specific integrated circuit (ASIC) compatible with shorter signals is needed for the Cherenkov detectors. One option is to test the functionality and performance of the SPACIROC3 with faster signals and possibly at a higher clock speed. We will evaluate this and other available ASICs to develop a full imaging focal surface that ideally would include timing resolution. A proto-type of the concept will be developed and tested in the laboratory. If successful, it will be flown on the test flight as part of the focal surface. Further plans for development will be formed after completing this stage.

7. Mission operations

The EUSO-SPB2 flight includes both local and remote operations. The field team will carry out final integration and check-out of the instrument at the launch site and commence operations once launch occurs. Remote communication between the science team and the CSBF command center will be through a server located at CSBF and used for transferring data. Progress of the flight will be monitored at the science team home stations with commanding originating from the Science Operation Center (SOC) at Colorado School of Mines. The science team will provide input for the observation plan based on data from operational weather satellites and forecasting. The SOC will also serve as the data archive during the mission. The processed data, along with the publications generated by this investigation, will be archived according to the Data Management Plan.

III. SIMULATION AND ANALYSIS SOFTWARE

For the EUSO-SPB2 project, we are employing two independent simulation and reconstruction packages, one called Offline [126, 127] and the other known as ESAF (EUSO Simulation and Analysis Framework) [128]. Both of these packages support development of event simulation and reconstruction. Most importantly, the detailed simulation capacity of these codes will be employed early on in the EUSO-SPB2 project to refine the final instrument design.

Offline was originally developed for the Pierre Auger Observatory [129], but has since been adapted to the needs of EUSO and associated pathfinders. ESAF was specifically designed for EUSO and its pathfinders. These codes are used to simulate the cosmic ray shower development in the atmosphere, the production of fluorescence and Cherenkov photons, and their propagation up to the detector. In both frameworks the various EUSO pathfinders are implemented and are used to simulate the detector response. The two frameworks also contain algorithms for reconstruction of data gathered by the pathfinders. We feel it is quite advantageous to have two simulation and reconstruction packages available, as it affords an opportunity for detailed cross-checks and ensures EUSO performance estimates are reliable.

The Offline software, has been used for simulation and reconstruction for the Auger Observatory since the first physics results were published in 2004. At the time of writing the software comprises some 360 000 lines of code and 35 000 lines of configuration information, representing a roughly 100 person-year investment according to the Constructive Cost Model [130].

Offline includes the latest fluorescence and Cherenkov light-yield models [131] atmospheric models and interfaces to many air shower simulation packages, including AIRES [132], CORSIKA [133], SENECA [134] and CONEX [123]. As Auger analyses using fluorescence measurements are quite mature at this point, the simulation algorithms have been well vetted with real data. For realistic Monte Carlo simulation (and real data analysis), the Offline code provides simple access to a collection of databases in which atmospheric monitoring data from a variety of sources can be stored. Raytracing in the

optical systems is performed using Geant4 [135]. Electronics and noise simulations can be performed using parametric models or from field measurements of the instrument in question. Several algorithms prepared by different teams have been developed to perform shower reconstruction.

The Offline framework provides many utilities and conveniences, to be discussed later, which have been exercised for over a decade by a large collaboration conducting data analysis. Furthermore, parts of the Offline framework have been adopted by other collaborations, including CODALEMA [136], TUNKA [137], HAWC [138], LOFAR [139] and NA61/SHINE [140, 141], allowing for mutually beneficial collaboration among scientists working on different experiments. The Offline framework is freely available upon request and is distributed under an open source BSD license [142].

The ESAF package was specifically designed for the performance assessment of space based cosmic ray observatories. It was developed in the framework of the EUSO mission [128] during the ESA phase A study. This software has been written mainly in C++ and makes use of the ROOT package [143]. The software was developed following an object oriented approach and is structured in a modular way.

The compilation of the ESAF software produces two distinct executable files called respectively Simu and Reco. The first one performs the simulation of the entire physical process from shower to telemetry. In this context, several air shower generators like SLAST [144], CONEX [123], CORSIKA [133] and others are available for use. An atmospheric model according to the 1976 Standard US Atmosphere [145] is implemented as well as different parameterizations for Fluorescence and Cherenkov yield. Both the NKSA [146] and the KLNOTU [147] fluorescence yield models have been implemented in the software. Standard Cherenkov theory is used in the ESAF computations of Cherenkov light emission. The Rayleigh scattering and ozone absorption processes are simulated in ESAF by means of the LOWTRAN 7 [148] atmosphere software. Several versions of the optics Monte Carlo simulator, developed at RIKEN (RIKEN ray trace code) have been interfaced with ESAF. The optics simulators for all the pathfinders like EUSO-TA, EUSO-Balloon, EUSO-SPB, and Mini-EUSO have been implemented and tested in ESAF. All the space-based detectors like TUS, K-EUSO and JEM-EUSO (in several configurations) are available. In addition, a GEANT 4 optics interface and a parametrical optics simulator are implemented. Both the PMT and the EC electric signal treatment is performed in a parametrical way. The last part of the simulation chain consists of the trigger sequence. A multiple stage trigger scheme is implemented in ESAF in order to maximize the ratio of real events to background. Once the trigger sequence has been applied the Simu executable produces an output ROOT file.

The Reco executable activates the reconstruction chain. If the event has been selected by the trigger algorithms, the first task is the recognition of pixel-GTUs with signal within the detector response table. Several algorithms have been implemented for this purpose.⁴ Once a clear shower-like pattern has been identified several time and space fits are performed for the arrival direction recognition. Eventually, the profile reconstruction

⁴ A gate time unit (GTU) = 2.5 μ s.

is performed in order to fit the X_{\max} and energy of the shower.

A. Offline design

The Offline framework comprises a collection of physics algorithms contained in *modules*; a *RunController* which commands the modules to execute in a particular sequence; a read/write *Event Data Model* from which modules read information and to which they write their results; a *Detector Description* which provides an interface to conditions data, such as detector calibration, performance and atmospheric conditions; and a *CentralConfig* which directs the modules and framework components to their configuration data and which tracks provenance. The general scheme is illustrated in Fig. 16, and discussed in more detail below.

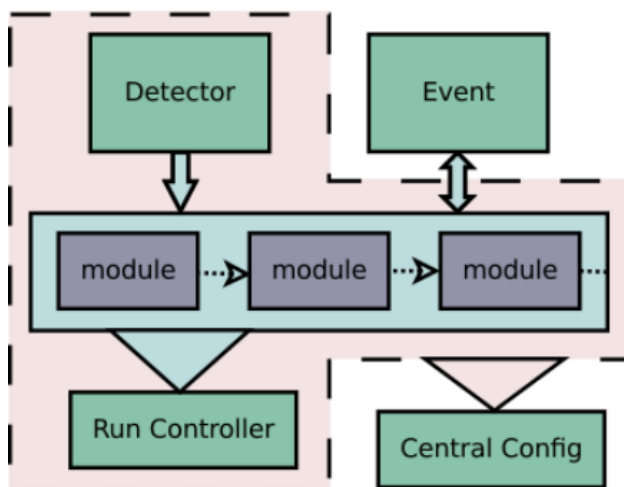


FIG. 16: General organization of the Offline framework. See the text for detailed explanation.

Simulation and reconstruction tasks are factorized into sequences of processing steps which can be simply pipelined. Physicists prepare processing algorithms in *modules*, which they register with the Offline framework via a one-line macro. This modular design facilitates comparison of algorithms and building a variety of applications by combining modules in various sequences. One can, for instance, very easily swap out a module for reading in simulated showers with a module to simulate laser shots in the instrument FoV. Control of module sequences is implemented with a *Run Controller*, which directs module execution according to a set of user provided instructions. We devised an XML-based language as one option for specifying sequencing instructions; this approach has proved sufficiently flexible for the majority of our applications, and it is simple to use, though a Python-based module control is also possible.

The Offline framework includes parallel hierarchies for accessing data: the *detector description* for retrieving conditions data, including detector geometry, calibration constants and atmospheric conditions; a plug-in mechanism in the atmosphere description

allowing various techniques for computing fluorescence and Cherenkov yields, both from parametric models and from measurements stored in databases; and an *event data model* for reading and writing information that changes for each event.

The detector description provides an interface from which module authors can retrieve the conditions data. Data requests are relayed to a back-end comprising a registry of so-called *managers*, each of which is capable of extracting a particular sort of information from various data sources. The manager mechanism is configurable and relieves authors of the physics code from having to deal with the details of selecting and decoding the correct data source. Managers are arranged in a “chain of responsibility” such that if an upstream manager cannot answer a request, it is passed along to downstream managers for another try.

The event data model contains raw, calibrated, reconstructed and Monte Carlo information, and serves as the backbone for communication between modules. The event is instrumented with a protocol allowing modules to discover its constituents at any point in processing, and thereby determine whether the input data required to carry out the desired processing are available. Offline is also equipped to read formats employed by the most popular air shower simulation packages [132, 133].

The Offline framework includes a system to organize and track data used to configure the software for different applications as well as parameters used in the physics modules. The *Central Config* configuration tool points modules and framework components to the location of their configuration data, and connects to Xerces-based [149] XML parsers to assist in reading information from these locations. We have wrapped Xerces with our own interface which provides ease of use at the cost of somewhat reduced flexibility, and which also adds functionality such as automatic units conversion and casting to various types, including commonly used container types.

The *Central Config* keeps track of all configuration data accessed during a run and stores them in an XML log file, which can be subsequently used to reproduce a run with an identical configuration. This allows collaborators to exchange configuration data for comparing results. The logging mechanism is also used to record the versions of modules and external libraries which are used for each run.

Syntax and content checking of the configuration files is implemented using W3C XML Schema validation [150]. Schema validation is used not only for internal configuration prepared by framework developers, but also to check the contents of physics module configuration files. This approach reduces the amount of code users and developers must prepare, and supports very robust checking.

As in many large software projects, each low level component of the Offline framework is verified with a small test program, known as a *unit test*. We have adopted the CppUnit testing framework [151] to help with implementing these tests. In addition to unit tests, a set of higher level acceptance tests has been developed which is used to verify that complete physics applications continue to function as expected, within some tolerance, during ongoing development. We employ a BuildBot system [152] to automatically compile the Offline software, run the unit and acceptance tests, and email developers in case of problems. The BuildBot runs each time the software repository is modified.

The Offline build system is based on the CMake cross-platform build tool [153], which has proven adequate to manage this project. In order to ease installation of Offline and its external dependencies, we have adopted a tool known as APE (Auger Package and Environment) [154]. APE is a dependency resolution engine co-developed by the Auger and HAWC collaborations. It automatically downloads a vetted combination of external packages required by Offline, builds them in whatever native build system applies for each package, and sets up the user's environment accordingly. APE is freely available, and used by the NA61/SHINE Collaboration, as well as Auger and HAWC.

B. ESAF design

The ESAF simulation code is structured in several independent modules the higher of which is the so called *SimuApplication*. An instance of this class is created in the *simu_main.cc* file where the method *SimuApplication::DoAll()* is called. This method performs the iterative call of the *SimuApplication::DoEvent()* method which takes care of the entire physical process on a single event basis. Such a method will create an instance of the *LightToEuso* class which executes the entire process from primary particle to photons on pupil. Several choices are available on which simulator is to be used but the default option is the so called *StandardLightToEuso* class. By calling the *StandardLightToEuso::Get()*, the virtual *Get()* methods of the shower generator, of the light production and transport will be called. Each one of the mentioned *Get()* methods will deliver output objects describing the shower profile, photons in atmosphere and photons on pupil. The choice of the object oriented approach shows its power here where the call of several polymorphic *Get()* methods allows great flexibility.

Always inside the *SimuApplication::DoEvent()* method the virtual *Detector::Get()* method will be called. This method takes care of the entire detector simulation. Several choices are open at this stage between various detector configurations. The most important of them can be considered to be the *EusoDetector*, (activating the RIKEN ray trace code), the *G4Detector* (activating the Geant 4 optics) and other testing or debugging detector simulators. Calling one of the above described methods will activate both optics and electronics simulators. As final output of the entire procedure a *Telemetry* object is produced.

The reconstruction procedure is activated in the *reco_main.cc* file. Here an instance of the *RecoFramework* class is created and the method *RecoFramework::Execute()* is called. While in the constructor function *RecoFramework::RecoFramework()* the module chain is built, the *RecoFramework::Execute()* method performs the entire sequence of calls to reconstruct the event. In fact, the module sequence is first initialized through an iterative call of the *ModuleFactory::MakeModule()* method which allocates all the *RecoModule* objects requested by parameter files. A *vector* named *fModules* with all the pointers to the created *RecoModule* objects is created. In the *RecoFramework::Execute()* method all the modules (which inherit from *RecoModule*) are initialized, called and cleared. Eventually all the output data are saved in the ROOT file. For performing all the mentioned operations, the polymorphic methods *RecoModule::PreProcess()*, *RecoModule::Process()*, *RecoModule::PostProcess()* and *RecoModule::SaveRootData()* are declared in each module. Each

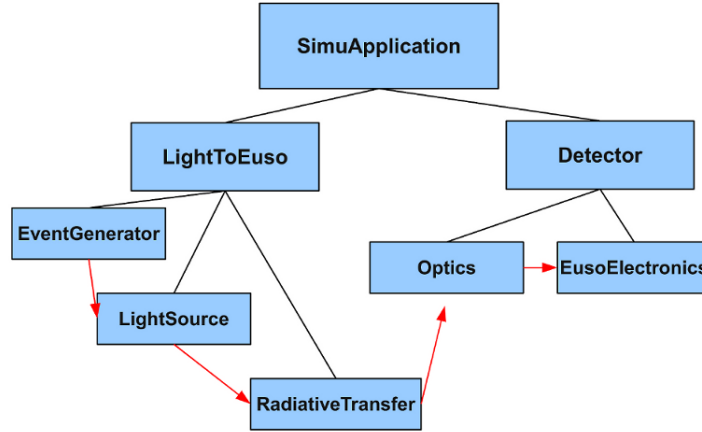


FIG. 17: a schematic view of the ESAF Simu application structure. The main application is the so called *SimuApplication*. The *LightToEuso* application takes care of all the physical process from shower to detector. The *EusoDetector* application performs the simulation of optics and electronics.

module has a specific function which can be either pattern recognition, direction fitting, profile reconstruction or X_{\max} and energy reconstruction. Several modules have been implemented in the course of the years but the most actual and currently updated are the *LTTPreClustering* and *PWISE* for the pattern recognition, the *TrackDirection2* for the direction reconstruction and the *PmtToShowerReco* for the energy reconstruction. A schematic view of the above mentioned structure is shown in Figs. 17 and 18.

C. Use of Offline and ESAF for EUSO pathfinders

Both the Offline and the ESAF packages were designed to allow a great deal of flexibility and to easily change the detector configuration. This flexibility made it relatively straightforward to use the codes for the various EUSO pathfinders. Both packages have been used for simulation and reconstruction of data for the EUSO-Balloon detector [155], the EUSO-TA [156] instrument as well as for simulation of the pending mini-EUSO and SPB missions [158, 159].

A EUSO pathfinder was flown aboard a balloon on August 2015 from the Timmins Stratospheric Balloon Facility in Ontario. During this flight, the instrument recorded data for about 5 hours. A laser and flasher were carried aboard a helicopter which flew beneath the balloon payload to test the instrument.

The Offline software was used to simulate the instrument and to reconstruct data taken during the flight. Figure 19 contains an image of a flasher and laser shot fired across the field of view of the payload. Figure 19 also shows the zenith angle distribution of reconstructed laser shots gathered during the campaign. As expected, the distribution peaks near 90° as the laser was shot horizontally across the downward pointing telescope.

Similar studies were performed using the ESAF package, including simulation of the

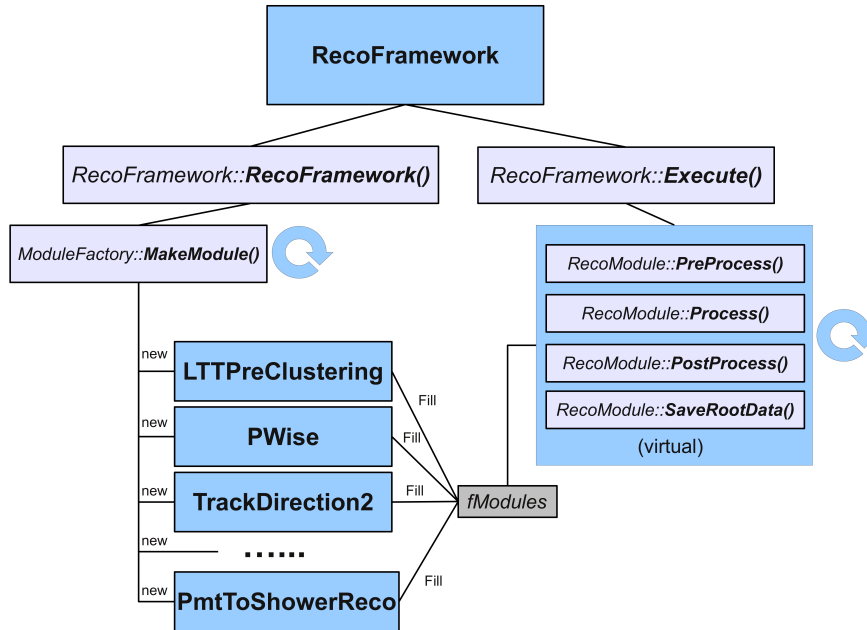


FIG. 18: A sketch of the reconstruction framework. The main application *RecoFramework* calls iteratively the *MakeModule* method which allocates all the required modules. A *vector* of pointers to the allocated objects is saved under the name *fModules*. In the *Execute* method the operations of all the modules are performed. All the modules are inheriting from the *RecoModule* class. The virtual methods *PreProcess*, *Process*, *PostProcess* and *SaveRootData* are called for all the allocated modules. Note that blue boxes represent classes, blue-gray boxes methods, the gray box is a C++ *vector* and the circular arrow indicates iterative repetition of some method or sequence of methods.

EUSO-Balloon response and detailed study of trigger performance. For instance, description of the simulation and reconstruction procedure used to predict the reconstruction performance is detailed in [160].

The EUSO-TA [156] pathfinder measurements were also simulated and reconstructed in a joint effort using both the Offline and ESAF packages [157]. In this experiment, the Black Rock Mesa TA (BRM-TA) telescopes were used to trigger a EUSO prototype instrument when an air shower was detected. Data recorded by the BRM-TA instrument were then used to reconstruct the shower distance, angle and energy. The simulation packages were then used to generate showers with the appropriate parameters to reproduce the EUSO-TA detected signal. The mapping of the real detector was introduced in both Offline and ESAF in order to take into account for the different efficiency of the pixels and for the dead PMTs. Figure 5 shows a comparison of a measurement and simulation of an air-shower recorded by EUSO-TA on 13 May 2015 [157]. Several test sources like stars, flashers and laser shots were implemented in the packages in order to validate the detector response and check reconstruction.

A simulation for the upcoming EUSO-SPB flight has also been prepared, as well as

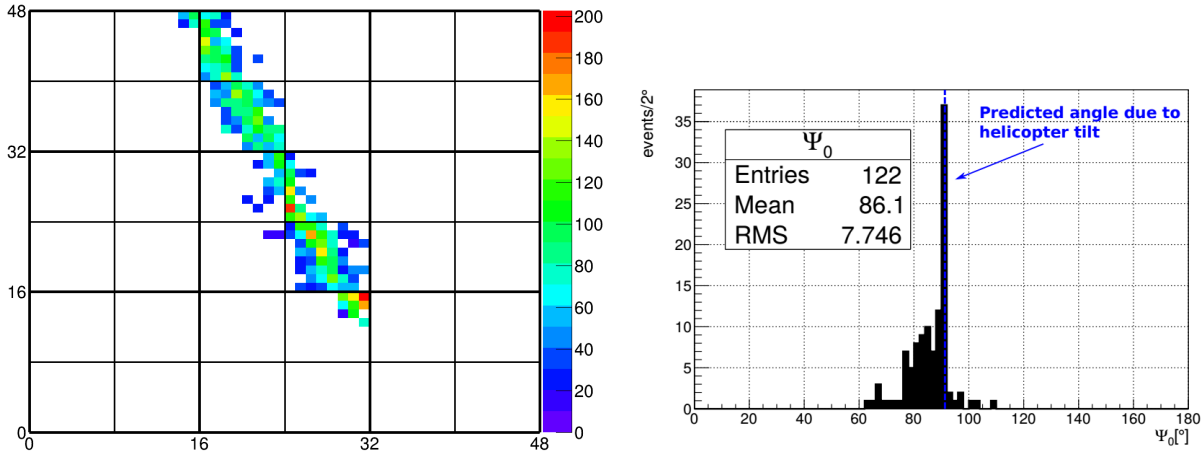


FIG. 19: *Left.* Focal surface image of a flasher and laser shot taken during the 1st stratospheric EUSO balloon flight as reconstructed using the Offline software. The horizontal and vertical axes label the pixel number, and the color indicates the number of flash ADC counts. The image is integrated over all of the time gates (2.5 microseconds each) for which flasher or laser data appeared to be present. *Right.* Zenith angle of reconstructed laser tracks fired across the EUSO-Balloon field of view.

the codes to read the data. A campaign of laser shots were reconstructed in Offline. Figure 20 depicts a Geant4 [135] simulation of the nominal EUSO-SPB design employing 3 lenses, and illustrates the ray tracing of a few photons entering the telescope. In these simulations, we re-implemented the native Geant4 modules which handle Fresnel reflections, total internal reflection, and reflections from ground or painted surfaces. This re-implementation was conducted in order to search for possible artifacts on the focal surface resulting from reflections in the optical system, and serves as a very convenient debugging tool. Figure 20 depicts images with reflections turned on and reflections turned off.

In Fig. 21 we show a simulation of a 10^{11} GeV air shower image on the EUSO-SPB focal surface, integrated over 127 GTUs.

A very comprehensive study on the expected trigger rate was performed with ESAF. The efficiency of the trigger has been studied in different cloud conditions, background, altitude and detector configurations [160]. A study of the cloud coverage and moon phase expected at the latitude and in the season where the balloon will fly has been performed [161]. We estimated the number of detectable particles to be between roughly 5 and 11 events depending on conditions the feasible SPB flight durations. As in the EUSO-Balloon case, we tested the energy reconstruction performance and estimated the fraction of reconstructable events.

Simulations for Mini-EUSO have also been implemented in both Offline and ESAF. Using ESAF, we found that the energy threshold is over 10^{12} GeV [162]. Furthermore we tested the response of the detector to meteors, Transient Luminous Events (TLEs), lightnings, space debris and planes. The trigger scheme has been tested on slow-moving

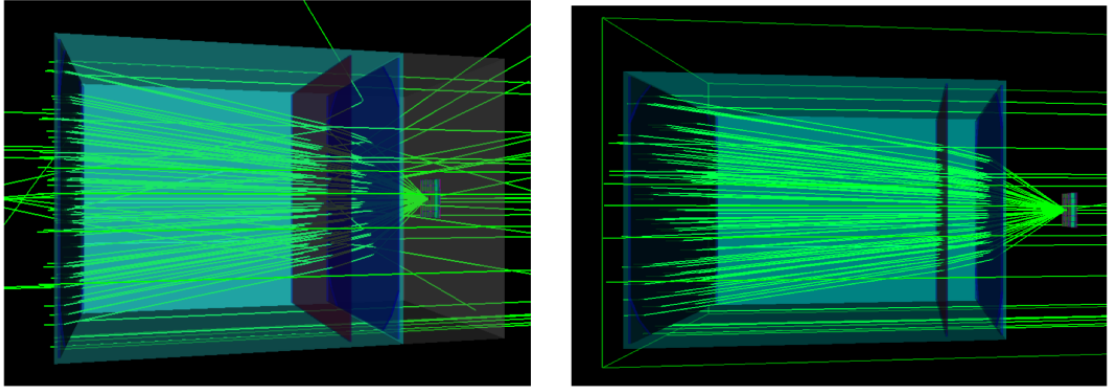


FIG. 20: EUSO-SPB simulated in Geant 4. *Left.* Parallel rays focusing on the Photo Detector Module (PDM). In this case reflections are included in the simulation. *Right.* Same situation with all reflections switched off. Note that the center (diffractive) lens may not actually be flown on the EUSO-SPB flight due to excessive photon absorption.

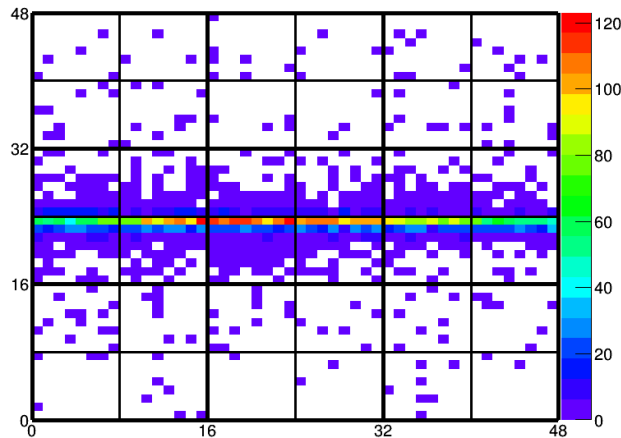


FIG. 21: Simulated 10^{11} GeV shower at a zenith angle of 50° as seen on the EUSO-SPB focal surface. The signal is integrated over 127 GTUs. No noise is included in this particular simulation.

events, relevant, for instance, for meteor detection. The Mini-EUSO trigger scheme is being tested on a wide range of events of different times scale and sizes.

D. EUSO-SPB2

Developing tools for simulation and reconstruction of a variety of instruments within the same overarching software framework is challenging. Fortunately, a large amount of the code developed so far can be straightforwardly recycled for use by EUSO-SPB2. It will (of course) be necessary to update the modules to model the new optical systems and electronics of SPB2, but the existing code provides an excellent opportunity to leverage

a great deal of previous development effort. The adaption of both ESAF and Offline to the needs of EUSO-SPB2 is underway. Both of these packages will be employed for simulations in early phases of the EUSO-SPB2 project in order to refine design of the final instrument. Indeed, preliminary tests are now being carried out to assess the capability to detect the direct Cherenkov light and the fluorescence light from distant events. Again, the two packages will be used to cross-check one another. We have begun developing a pipeline to simulate the Cherenkov signal resulting from ν_τ 's skimming the Earth and producing τ leptons which generate upgoing showers [163].

IV. EXPECTED PERFORMANCE

A. Duty cycle

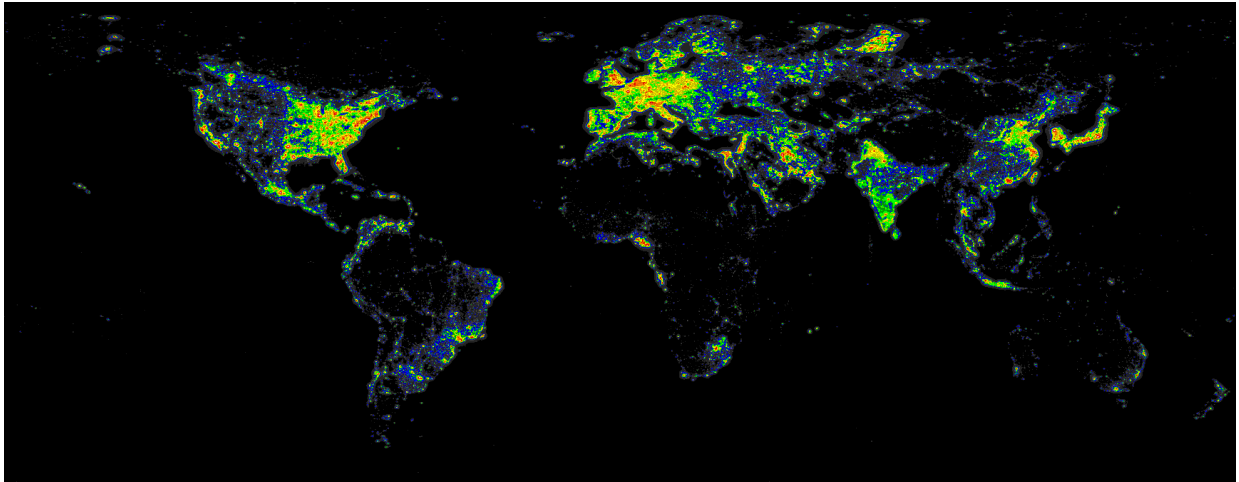


FIG. 22: Light pollution heat map of the world [164].

EUSO-SPB2 observations can only be done on clear moonless nights. The balloon will fly in the Southern hemisphere and thus subject to less light pollution than if it were exposed to the Northern hemisphere, see Fig. 22. A thorough study suggests that a 50 day flight launched at Wanaka latitude of 45° S and about the expected time of EUSO-SPB (March/April) would see between 190 and 260 hr of dark time, depending on when the launch happens relative to the moon phase [159]. For a 100 day flight, the fluctuations would smooth out a bit, and hence we estimate 500 hr would be a realistic number of dark hours, with no moon and between the end and start of astronomical twilight at 33 km. Relative to a detector on ground, there is a loss of about 50 minutes per day because the horizon is further away and this loss factor is included. Then, 500 hr/2400 hr yields a 20.8% duty cycle. Since the SPBs from Wanaka go east, there is a jet lag effect that reduces the 500 hr by a few percent. We account for this correction by taking a duty cycle $\delta \approx 0.2$. This estimate does not take into account possible reduction of the duty cycle due to obscuration by clouds, and further assumes an operationally perfect detector. In

our calculations we account for the effect of cloud obscuration by introducing a scaling factor κ , which combines the trigger effects and reconstruction efficiency in the presence of clouds, as well as the fraction of time during which data are taken in clear and cloudy conditions; namely, if the entire data sample were to be taken in clear sky conditions we have $\kappa = 1$. Preliminary ESAF studies for EUSO-SPB suggest that $\kappa \approx 0.75$ [160, 161]. Since roughly 2/3 of the time the FoV will be obscured by clouds, the previous κ estimate indicates that half of the events obscured by clouds can be considered of sufficient quality to have the same reconstruction and trigger efficiency as clear sky conditions. This agrees with previous studies for the JEM-EUSO mission [165–168]. To estimate the event rate for EUSO-SPB2 we conveniently define an effective duty cycle $\delta_{\text{eff}} = \delta \kappa \approx 0.15$.

B. Event rates

By comparing the red and blue lines in the left panel of Fig. 2 one can discern that the number of events detected via Cherenkov radiation, in the range $10^7 < E/\text{GeV} < 10^8$, would be around 1,000 for a 100 day mission. There may be small variations in this ratio arriving from the effective duty cycle achieved by the instrument.

The final configuration for the EUSO-SPB2 fluorescence detector will depend on the performance of EUSO-SPB. Therefore, we cannot yet derive with certainty the expected rate of UHECR events. Obviously, we expect EUSO-SPB2 to perform better than EUSO-SPB. In the following we provide a rough estimate of the number of events using the expected EUSO-SPB performance as a guideline.

1. Estimate of UHECR events using ESAF

We estimated the event rate of EUSO-SPB with ESAF taking into account clear and cloudy sky conditions, and the effect of Cherenkov reflection from high level clouds [161, 162]. As an illustration, in Fig. 23 we show the expected number of triggered events as a function of $\log(E)$, for clear sky conditions. Taking into account the reconstruction efficiency $\epsilon \sim 0.6$ and correcting by the κ factor due to obscuration by clouds, we find that for a flight with 138 hr of dark time, we expect 6.3 ± 0.9 events, whereas for a flight of 211 hr of dark time, we expect 10.6 ± 2.3 events.

2. Estimate of UHECR event rates using CONEX + Offline

The expected number of detectable UHECR events has also been estimated by Monte Carlo techniques using CONEX [123] to simulate shower development and Offline to simulate the detector response. The results from these simulations for various pseudo-triggers are shown in Fig. 24.

A laser campaign was performed to assess the trigger threshold for EUSO-SPB. The results of this campaign indicate that a 100% trigger efficiency requires a pseudo-trigger with 500+ photons at the EUSO-SPB aperture per GTU, for 5 GTUs. However, using

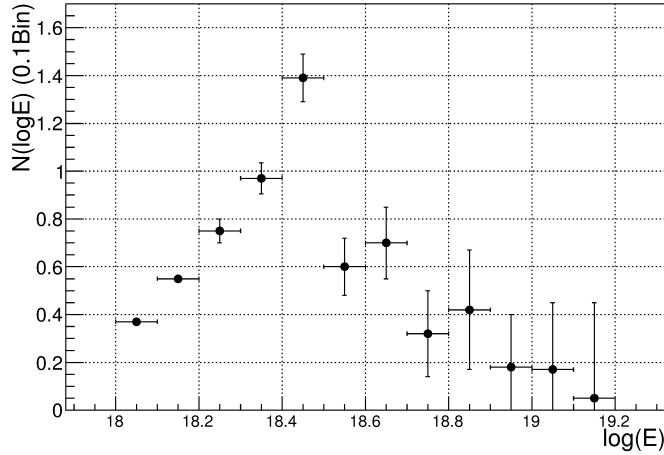


FIG. 23: Spectrum of triggered events for 118 hr flight as would be detected by EUSO-SPB in clear sky conditions.

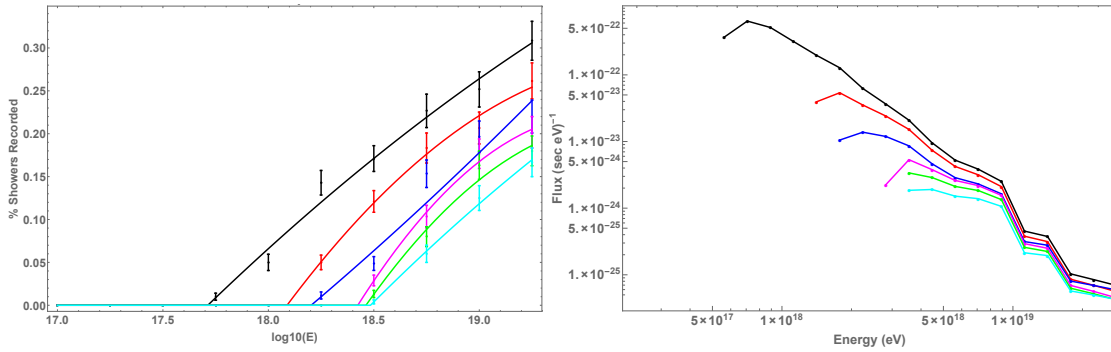


FIG. 24: *Left.* The fraction of observable extensive air showers relative to the number simulated events for different photon thresholds: 100+ photons/GTU, 200+ photons/GTU, 300+ photons/GTU, 400+ photons/GTU, 500+ photons/GTU, and 600+ photons/GTU. *Right.* The flux of extensive air showers observable by EUSO-SPB for the various photon thresholds [169].

the flux curve for the 500+ photons/GTU threshold alone does not fully capture how many events EUSO-SPB might record. This is because 400+ photons/GTU corresponds to an 85% triggering efficiency, whereas 300+ photons/GTU corresponds to 22% triggering efficiency. The 200+/GTU and 100+/GTU pseudo-triggers are satisfied only by laser energies that did not trigger during the field tests. Therefore, the total flux curve would be the sum of the 500+ photons/GTU curve, the portion of the 400+ curve not captured by the 500+ curve scaled by 0.85, and the portion of the 300+ curve not captured by the 400+ curve scaled by 0.22. A plot of the estimated total flux for EUSO-SPB is exhibited in Fig. 25.

The flux curves shown in Figs. 24 and 25 can be integrated to estimate the expected trigger rate. The results of these integrations are given in Table. II and can be summarized

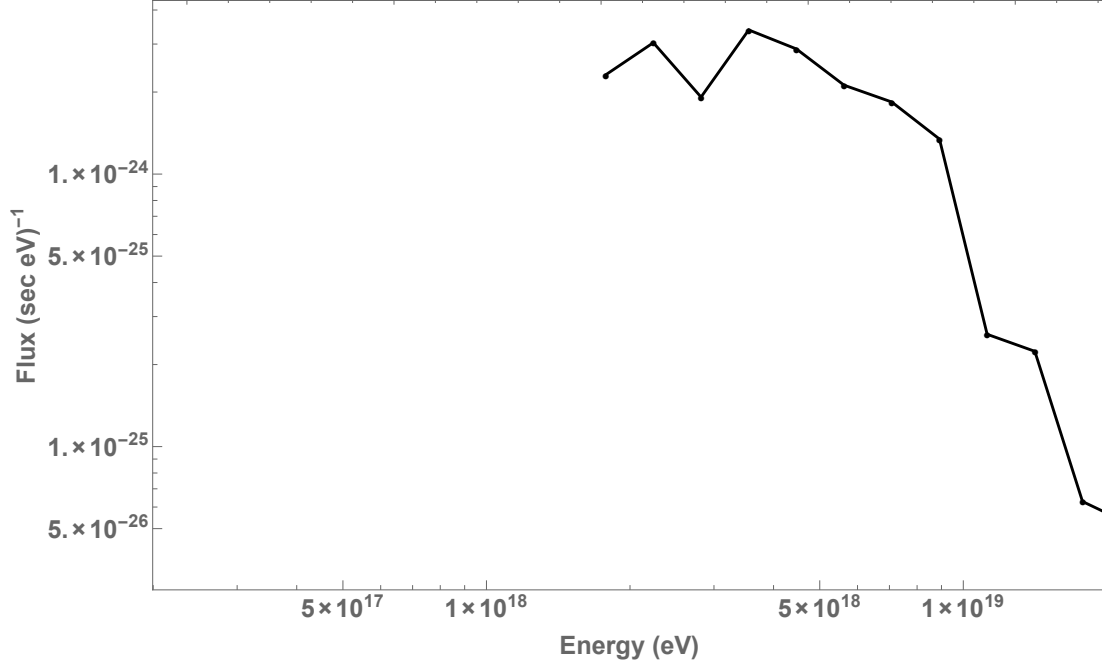


FIG. 25: Summation of flux curves shown in Fig. 24 with corresponding trigger efficiency [169].

as follows: we expect 4.5 triggered events per 55 hours of operation, with an energy threshold at about $10^{9.7}$ GeV and a photon threshold of 500 to 600 photons/GTU. This corresponds to a trigger event rate $n_{\text{tr}} = 0.081 \text{ hr}^{-1}$.

As discussed above independent estimates of the trigger rates have been performed including the effect of clouds of varying altitude and thickness (in ESAF) and assuming a clear sky (in both ESAF and Offline). Using the ESAF reconstruction efficiency we can now translate the CONEX + Offline trigger rate into a rate of reconstructed events, $n_{\text{re}} = n_{\text{tr}} \epsilon \sim 0.0486 \text{ hr}^{-1}$. Moreover, using the ESAF κ scaling factor we can take account of cloud obscuration, and for a 138 dark hour flight we expect a total of about 5 events to be reconstructed. Note that this agrees with the estimate based solely on ESAF simulation at the 1σ level.

For EUSO-SPB2, it is likely the photon threshold will be improved by about a factor of 2 compared to EUSO-SPB. The argument for this is as follows. The mirrors should deliver about twice as much light to the focal surface as the EUSO-SPB lens system, and the spot size should cover about 2 pixels rather than 4-6 pixels. EUSO-SPB has roughly a threshold of 500 photons/GTU and 40 photons from background, which yields 50 counts/GTU from signal and 4 counts/GTU from background, assuming 0.1 overall efficiency. Doubling the throughput of the optical system would yield 100 counts/GTU from signal but still 4 counts from background (2 pixels multiplied by 2 counts/pixel). This would imply an improvement on the trigger rate by factor of 2. As the EUSO-SPB2 FoV could be $3.2^\circ \times 28.8^\circ$ (as opposed to the $12^\circ \times 12^\circ$ FoV for EUSO-SPB), the trigger rate will also increase by a factor of 2.5 for showers of interest. With this in mind, the number of reconstructed events

TABLE II: Expected UHECR event rate for EUSO-SPB using various pseudo-triggers. The row highlighted in green corresponds to the nominal event rate estimated in [170]. The rows highlighted in blue show the expected event rates for two possible pseudo-triggers with 100% efficiency. The last row, highlighted in red, indicates the best estimate, including the different trigger efficiencies [169].

trigger threshold (photons/GTU)	event/hr	event/night	event/week
100	2.300 ± 0.005	18.1 ± 0.04	127.0 ± 0.3
200	0.430 ± 0.020	3.40 ± 0.10	24.0 ± 1.0
300	0.180 ± 0.010	1.40 ± 0.08	10.0 ± 0.6
400	0.089 ± 0.008	0.71 ± 0.07	5.0 ± 0.5
500	0.065 ± 0.007	0.52 ± 0.05	3.7 ± 0.4
600	0.047 ± 0.005	0.37 ± 0.04	2.6 ± 0.3
complete	0.081 ± 0.010	0.64 ± 0.08	4.5 ± 0.6

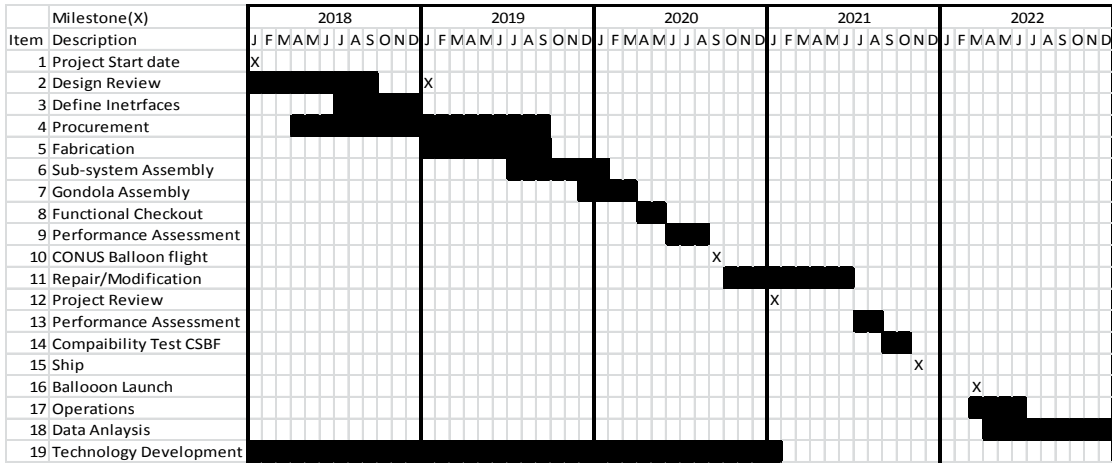


FIG. 26: Development schedule for EUSO-SPB2.

in a $T \sim 100$ day mission, which will be useful for physics analysis, is found to be

$$N_{re} = 5 n_{tr} \epsilon \delta_{eff} T \sim 87. \quad (3)$$

All in all, we expect a sample size sufficient to perform interesting analysis.

V. DEVELOPMENT SCHEDULE AND DATA MANAGEMENT

A Gantt chart showing the development schedule is shown in Fig. 26.

Low-level processing: The Offline and ESAF software packages will be used to reconstruct events recorded by EUSO-SPB2, classify and reject the majority of events that are

of no scientific value. At this stage, preliminary calibrations will have been applied, but not corrections for atmospheric conditions. This allows the flexibility to make a revision of the Level 2 files later, without repeating Level 1 processing.

Higher level processing: Physically meaningful data such as arrival directions, energies, and background estimates will be extracted from the data sample using Offline and ESAF, and refined later using atmospheric and calibration databases validated or developed from observational data. In addition to these Level 2 data, we will produce a Level 3 product containing an exposure and efficiency map. This will allow scientists outside the core team to investigate the data.

Software and Data Archiving and Release: The EUSO US Data Center located at the SOC will have a Redundant Array of Independent Disks (RAID) for storage of Level 1-3 software. After approximately a 1 year period for calibration of data analysis, Level 2 data files and Level 3 products will be delivered to the scientific community along with software and documentation required to perform analysis.

-
- [1] A. Neronov, D. V. Semikoz, I. Vovk and R. Mirzoyan, *Cosmic-ray composition measurements and cosmic ray background-free γ -ray observations with Cherenkov telescopes*, Phys. Rev. D **94**, 123018 (2016) doi:10.1103/PhysRevD.94.123018 [arXiv:1610.01794 [astro-ph.IM]].
 - [2] A. Neronov, D. V. Semikoz, L. A. Anchordoqui, J. Adams and A. V. Olinto, *Sensitivity of a proposed space-based Cherenkov astrophysical-neutrino telescope*, Phys. Rev. D **95**, 023004 (2017) doi:10.1103/PhysRevD.95.023004 [arXiv:1606.03629 [astro-ph.IM]].
 - [3] A. Aab *et al.* [Pierre Auger Collaboration], *Testing hadronic interactions at ultrahigh energies with air showers measured by the Pierre Auger Observatory*, Phys. Rev. Lett. **117**, 192001 (2016) doi:10.1103/PhysRevLett.117.192001 [arXiv:1610.08509 [hep-ex]].
 - [4] F. W. Stecker, J. F. Krizmanic, L. M. Barbier, E. Loh, J. W. Mitchell, P. Sokolsky and R. E. Streitmatter, *Observing the ultrahigh-energy universe with OWL eyes*, Nucl. Phys. Proc. Suppl. **136C**, 433 (2004) doi:10.1016/j.nuclphysbps.2004.10.027 [astro-ph/0408162].
 - [5] L. A. Anchordoqui, G. R. Farrar, J. F. Krizmanic, J. Matthews, J. W. Mitchell, D. Nitz, A. V. Olinto, T. C. Paul, P. Sokolsky, G. B. Thomson, and T. J. Weiler, *Roadmap for Ultra-High Energy Cosmic Ray Physics and Astronomy (whitepaper for Snowmass 2013)*, arXiv:1307.5312 [astro-ph.HE].
 - [6] 2011 NASA Strategic Plan. Available at:
<https://www.nasa.gov/pdf/516579main-NASA2011StrategicPlan.pdf>
 - [7] 2010 NASA Science Plan. (for the Science Mission Directory). Available at:
https://smd-prod.s3.amazonaws.com/science-green/s3fs-public/mnt/medialibrary/2010/08/30/2010SciencePlan_TAGGED.pdf
 - [8] *Connecting Quarks with the Cosmos: Eleven Science Questions for the New Century* Washington, DC. The National Academies Press, 2003. 1.
 - [9] <https://smd-prod.s3.amazonaws.com/science-pink/s3fs-public/atoms/files/secure-Astrophysics-Roadmap-2013.pdf>
 - [10] J. J. Beatty *et al.*, *Working Group Report: Cosmic probes of fundamental physics*,

- arXiv:1310.5662 [hep-ph].
- [11] T. Antoni *et al.* [KASCADE Collaboration], **KASCADE measurements of energy spectra for elemental groups of cosmic rays: Results and open problems**, *Astropart. Phys.* **24**, 1 (2005) doi:10.1016/j.astropartphys.2005.04.001 [astro-ph/0505413].
 - [12] J. Abraham *et al.* [Pierre Auger Collaboration], **Measurement of the energy spectrum of cosmic rays above 10^{18} eV using the Pierre Auger Observatory**, *Phys. Lett. B* **685**, 239 (2010) doi:10.1016/j.physletb.2010.02.013 [arXiv:1002.1975 [astro-ph.HE]].
 - [13] D. J. Bird *et al.* [HiRes Collaboration], **Evidence for correlated changes in the spectrum and composition of cosmic rays at extremely high-energies**, *Phys. Rev. Lett.* **71**, 3401 (1993) doi:10.1103/PhysRevLett.71.3401.
 - [14] R. U. Abbasi *et al.* [HiRes Collaboration], **First observation of the Greisen-Zatsepin-Kuzmin suppression**, *Phys. Rev. Lett.* **100**, 101101 (2008) doi:10.1103/PhysRevLett.100.101101 [astro-ph/0703099].
 - [15] J. Abraham *et al.* [Pierre Auger Collaboration], **Observation of the suppression of the flux of cosmic rays above 4×10^{19} eV**, *Phys. Rev. Lett.* **101**, 061101 (2008) doi:10.1103/PhysRevLett.101.061101 [arXiv:0806.4302 [astro-ph]].
 - [16] W. D. Apel *et al.*, **The spectrum of high-energy cosmic rays measured with KASCADE-Grande**, *Astropart. Phys.* **36**, 183 (2012). doi:10.1016/j.astropartphys.2012.05.023
 - [17] M. G. Aartsen *et al.* [IceCube Collaboration], **Measurement of the cosmic ray energy spectrum with IceTop-73**, *Phys. Rev. D* **88**, no. 4, 042004 (2013) doi:10.1103/PhysRevD.88.042004 [arXiv:1307.3795 [astro-ph.HE]].
 - [18] S. P. Knurenko, Z. E. Petrov, R. Sidorov, I. Y. Slepsov, S. K. Starostin and G. G. Struchkov, **Cosmic ray spectrum in the energy range $10^{15} - 10^{18}$ eV and the second knee according to the small Cherenkov setup at the Yakutsk EAS array**, arXiv:1310.1978 [astro-ph.HE].
 - [19] V. V. Prosin *et al.*, **Tunka-133: Results of 3 year operation**, *Nucl. Instrum. Meth. A* **756**, 94 (2014). doi:10.1016/j.nima.2013.09.018
 - [20] T. Abu-Zayyad *et al.* [HiRes-MIA Collaboration], **Measurement of the cosmic ray energy spectrum and composition from 10^{17} -eV to $10^{18.3}$ -eV using a hybrid fluorescence technique**, *Astrophys. J.* **557**, 686 (2001) doi:10.1086/322240 [astro-ph/0010652].
 - [21] D. R. Bergman and J. W. Belz, **Cosmic rays: The second knee and beyond**, *J. Phys. G* **34**, R359 (2007) doi:10.1088/0954-3899/34/10/R01 [arXiv:0704.3721 [astro-ph]].
 - [22] J. R. Hoerandel, **On the knee in the energy spectrum of cosmic rays**, *Astropart. Phys.* **19**, 193 (2003) doi:10.1016/S0927-6505(02)00198-6 [astro-ph/0210453].
 - [23] C. Patrignani *et al.* [Particle Data Group], **Review of Particle Physics**, *Chin. Phys. C* **40**, no. 10, 100001 (2016). doi:10.1088/1674-1137/40/10/100001
 - [24] D. Allard, E. Parizot, E. Khan, S. Goriely and A. V. Olinto, **UHE nuclei propagation and the interpretation of the ankle in the cosmic-ray spectrum**, *Astron. Astrophys.* **443**, L29 (2005) doi:10.1051/0004-6361:200500199 [astro-ph/0505566].
 - [25] D. Allard, E. Parizot and A. V. Olinto, **On the transition from galactic to extragalactic cosmic-rays: spectral and composition features from two opposite scenarios**, *Astropart. Phys.* **27**, 61 (2007) doi:10.1016/j.astropartphys.2006.09.006 [astro-ph/0512345].
 - [26] K. Greisen, **End to the cosmic ray spectrum?**, *Phys. Rev. Lett.* **16**, 748 (1966) doi:10.1103/PhysRevLett.16.748.

- [27] G. T. Zatsepin and V. A. Kuzmin, [Upper limit of the spectrum of cosmic rays](#), JETP Lett. **4**, 78 (1966) [Pisma Zh. Eksp. Teor. Fiz. **4**, 114 (1966)].
- [28] M. Hillas, [The energy spectrum of cosmic rays in an evolving universe](#), Phys. Lett. A **24**, 677 (1967) doi:10.1016/0375-9601(67)91023-7.
- [29] V. Berezhinsky, A. Z. Gazizov and S. I. Grigorieva, [On astrophysical solution to ultrahigh-energy cosmic rays](#), Phys. Rev. D **74**, 043005 (2006) doi:10.1103/PhysRevD.74.043005 [hep-ph/0204357].
- [30] K. H. Kampert and M. Unger, [Measurements of the cosmic ray composition with air shower experiments](#), Astropart. Phys. **35**, 660 (2012) doi:10.1016/j.astropartphys.2012.02.004 [arXiv:1201.0018 [astro-ph.HE]].
- [31] A. Aab *et al.* [Pierre Auger Collaboration], [Depth of maximum of air-shower profiles at the Pierre Auger Observatory I: Measurements at energies above \$10^{17.8}\$ eV](#), Phys. Rev. D **90**, no. 12, 122005 (2014) doi:10.1103/PhysRevD.90.122005 [arXiv:1409.4809 [astro-ph.HE]].
- [32] A. Aab *et al.* [Pierre Auger Collaboration], [Depth of maximum of air-shower profiles at the Pierre Auger Observatory II: Composition implications](#), Phys. Rev. D **90**, no. 12, 122006 (2014) doi:10.1103/PhysRevD.90.122006 [arXiv:1409.5083 [astro-ph.HE]].
- [33] A. Aab *et al.* [Pierre Auger Collaboration], [Evidence for a mixed mass composition at the ankle in the cosmic-ray spectrum](#), Phys. Lett. B **762**, 288 (2016) doi:10.1016/j.physletb.2016.09.039 [arXiv:1609.08567 [astro-ph.HE]].
- [34] A. Aab *et al.* [Pierre Auger Collaboration], [Combined fit of spectrum and composition data as measured by the Pierre Auger Observatory](#), [arXiv:1612.07155 [astro-ph.HE]].
- [35] P. Abreu *et al.* [Pierre Auger Collaboration], [Large scale distribution of arrival directions of cosmic rays detected above \$10^{18}\$ eV at the Pierre Auger Observatory](#), Astrophys. J. Suppl. **203**, 34 (2012) doi:10.1088/0067-0049/203/2/34 [arXiv:1210.3736 [astro-ph.HE]].
- [36] A. Aab *et al.* [Pierre Auger Collaboration], [Large scale distribution of ultrahigh energy cosmic rays detected at the Pierre Auger Observatory with zenith angles up to \$80^\circ\$](#) , Astrophys. J. **802**, no. 2, 111 (2015) doi:10.1088/0004-637X/802/2/111 [arXiv:1411.6953 [astro-ph.HE]].
- [37] R. U. Abbasi *et al.*, [Study of ultrahigh energy cosmic ray composition using Telescope Arrays Middle Drum detector and surface array in hybrid mode](#), Astropart. Phys. **64**, 49 (2014) doi:10.1016/j.astropartphys.2014.11.004 [arXiv:1408.1726 [astro-ph.HE]].
- [38] R. Abbasi *et al.* [Pierre Auger and Telescope Array Collaborations], [Report of the working group on the composition of ultrahigh energy cosmic rays](#), arXiv:1503.07540 [astro-ph.HE].
- [39] R. U. Abbasi *et al.* [Telescope Array Collaboration], [Indications of intermediate-scale anisotropy of cosmic rays with energy greater than 57 EeV in the Northern sky measured with the surface detector of the Telescope Array experiment](#), Astrophys. J. **790**, L21 (2014) doi:10.1088/2041-8205/790/2/L21 [arXiv:1404.5890 [astro-ph.HE]].
- [40] W. D. Apel *et al.*, [Ankle-like feature in the energy spectrum of light elements of cosmic rays observed with KASCADE-Grande](#), Phys. Rev. D **87**, 081101 (2013) doi:10.1103/PhysRevD.87.081101 [arXiv:1304.7114 [astro-ph.HE]].
- [41] R. Aloisio, V. Berezhinsky and P. Blasi, [Ultrahigh energy cosmic rays: implications of Auger data for source spectra and chemical composition](#), JCAP **1410**, no. 10, 020 (2014) doi:10.1088/1475-7516/2014/10/020 [arXiv:1312.7459 [astro-ph.HE]].
- [42] M. Unger, G. R. Farrar and L. A. Anchordoqui, [Origin of the ankle in the ultrahigh energy](#)

- cosmic ray spectrum, and of the extragalactic protons below it, *Phys. Rev. D* **92**, no. 12, 123001 (2015) doi:10.1103/PhysRevD.92.123001 [arXiv:1505.02153 [astro-ph.HE]].
- [43] N. Globus, D. Allard and E. Parizot, *A complete model of the cosmic ray spectrum and composition across the Galactic to extragalactic transition*, *Phys. Rev. D* **92**, no. 2, 021302 (2015) doi:10.1103/PhysRevD.92.021302 [arXiv:1505.01377 [astro-ph.HE]].
- [44] D. F. Torres and L. A. Anchordoqui, *Astrophysical origins of ultrahigh energy cosmic rays*, *Rept. Prog. Phys.* **67**, 1663 (2004) doi:10.1088/0034-4885/67/9/R03 [astro-ph/0402371].
- [45] K. Kotera and A. V. Olinto, *The astrophysics of ultrahigh energy cosmic rays*, *Ann. Rev. Astron. Astrophys.* **49**, 119 (2011) doi:10.1146/annurev-astro-081710-102620 [arXiv:1101.4256 [astro-ph.HE]].
- [46] P. L. Biermann and P. A. Strittmatter, *Synchrotron emission from shock waves in active galactic nuclei*, *Astrophys. J.* **322**, 643 (1987). doi:10.1086/165759
- [47] J. P. Rachen and P. L. Biermann, *Extragalactic ultrahigh-energy cosmic rays I: Contribution from hot spots in FR-II radio galaxies*, *Astron. Astrophys.* **272**, 161 (1993) [astro-ph/9301010].
- [48] A. Y. Neronov, D. V. Semikoz and I. I. Tkachev, *Ultra-high energy cosmic ray production in the polar cap regions of black hole magnetospheres*, *New J. Phys.* **11**, 065015 (2009) doi:10.1088/1367-2630/11/6/065015 [arXiv:0712.1737 [astro-ph]].
- [49] R. J. Moncada, R. A. Colon, J. J. Guerra, M. J. O'Dowd and L. A. Anchordoqui, *Ultra-high energy cosmic ray nuclei from remnants of dead quasars*, *JHEAp* (to be published) arXiv:1702.00053 [astro-ph.HE].
- [50] G. Cavallo, *On the sources of ultra-high energy cosmic rays*, *Astron. Astrophys.* **65**, 415 (1978).
- [51] G. E. Romero, J. A. Combi, L. A. Anchordoqui and S. E. Perez Bergliaffa, *A possible source of extragalactic cosmic rays with arrival energies beyond the GZK cutoff*, *Astropart. Phys.* **5**, 279 (1996) doi:10.1016/0927-6505(96)00029-1 [gr-qc/9511031].
- [52] A. Aab *et al.* [Pierre Auger Collaboration], *Searches for anisotropies in the arrival directions of the highest energy cosmic rays detected by the Pierre Auger Observatory*, *Astrophys. J.* **804**, no. 1, 15 (2015) doi:10.1088/0004-637X/804/1/15 [arXiv:1411.6111 [astro-ph.HE]].
- [53] L. A. Anchordoqui, G. E. Romero and J. A. Combi, *Heavy nuclei at the end of the cosmic ray spectrum?*, *Phys. Rev. D* **60**, 103001 (1999) doi:10.1103/PhysRevD.60.103001 [astro-ph/9903145].
- [54] P. Blasi, R. I. Epstein and A. V. Olinto, *Ultrahigh-energy cosmic rays from young neutron star winds*, *Astrophys. J.* **533**, L123 (2000) doi:10.1086/312626 [astro-ph/9912240].
- [55] K. Fang, K. Kotera and A. V. Olinto, *Newly-born pulsars as sources of ultrahigh energy cosmic rays*, *Astrophys. J.* **750**, 118 (2012) doi:10.1088/0004-637X/750/2/118 [arXiv:1201.5197 [astro-ph.HE]].
- [56] K. Fang, K. Kotera and A. V. Olinto, *Ultrahigh energy cosmic ray nuclei from extragalactic pulsars and the effect of their Galactic counterparts*, *JCAP* **1303**, 010 (2013) doi:10.1088/1475-7516/2013/03/010 [arXiv:1302.4482 [astro-ph.HE]].
- [57] K. Kotera, E. Amato and P. Blasi, *The fate of ultrahigh energy nuclei in the immediate environment of young fast-rotating pulsars*, *JCAP* **1508**, no. 08, 026 (2015) doi:10.1088/1475-7516/2015/08/026 [arXiv:1503.07907 [astro-ph.HE]].
- [58] M. Ackermann *et al.* [Fermi-LAT Collaboration], *GeV observations of star-forming*

- galaxies with *Fermi-LAT*, *Astrophys. J.* **755**, 164 (2012) doi:10.1088/0004-637X/755/2/164 [arXiv:1206.1346 [astro-ph.HE]].
- [59] L. A. Anchordoqui, H. Goldberg and D. F. Torres, *Anisotropy at the end of the cosmic ray spectrum?*, *Phys. Rev. D* **67**, 123006 (2003) doi:10.1103/PhysRevD.67.123006 [astro-ph/0209546].
- [60] L. A. Anchordoqui, T. C. Paul, L. H. M. da Silva, D. F. Torres and B. J. Vlcek, *What IceCube data tell us about neutrino emission from star-forming galaxies (so far)*, *Phys. Rev. D* **89**, no. 12, 127304 (2014) doi:10.1103/PhysRevD.89.127304 [arXiv:1405.7648 [astro-ph.HE]].
- [61] H. N. He, A. Kusenko, S. Nagataki, B. B. Zhang, R. Z. Yang and Y. Z. Fan, *Monte Carlo Bayesian search for the plausible source of the Telescope Array hot spot*, *Phys. Rev. D* **93**, 043011 (2016) doi:10.1103/PhysRevD.93.043011 [arXiv:1411.5273 [astro-ph.HE]].
- [62] D. N. Pfeffer, E. D. Kovetz and M. Kamionkowski, *Ultra-high-energy-cosmic-ray hot spots from tidal disruption events*, *Mon. Not. Roy. Astron. Soc.* **466**, 2922 (2017) doi:10.1093/mnras/stw3337 [arXiv:1512.04959 [astro-ph.HE]].
- [63] R. S. Nemmen, C. Bonatto and T. Storchi-Bergmann, *A correlation between the highest energy cosmic rays and nearby active galactic nuclei detected by Fermi*, *Astrophys. J.* **722**, 281 (2010) doi:10.1088/0004-637X/722/1/281 [arXiv:1007.5317 [astro-ph.HE]].
- [64] T. Piran, *Gamma-ray bursts and the fireball model*, *Phys. Rept.* **314**, 575 (1999) doi:10.1016/S0370-1573(98)00127-6 [astro-ph/9810256].
- [65] E. Waxman, *Cosmological gamma-ray bursts and the highest energy cosmic rays*, *Phys. Rev. Lett.* **75**, 386 (1995) doi:10.1103/PhysRevLett.75.386 [astro-ph/9505082].
- [66] M. Vietri, *On the acceleration of ultrahigh-energy cosmic rays in gamma-ray bursts*, *Astrophys. J.* **453**, 883 (1995) doi:10.1086/176448 [astro-ph/9506081].
- [67] N. Globus, D. Allard, R. Mochkovitch and E. Parizot, *UHECR acceleration at GRB internal shocks*, *Mon. Not. Roy. Astron. Soc.* **451**, no. 1, 751 (2015) doi:10.1093/mnras/stv893 [arXiv:1409.1271 [astro-ph.HE]].
- [68] N. Globus, D. Allard, E. Parizot and T. Piran, *Probing the extragalactic cosmic rays origin with gamma-ray and neutrino backgrounds*, arXiv:1703.04158 [astro-ph.HE].
- [69] R. W. Clay [for the Pierre Auger Collaboration], *The anisotropy search program for the Pierre Auger Observatory*, astro-ph/0308494.
- [70] L. A. Anchordoqui, M. T. Dova, L. N. Epele and S. J. Sciutto, *Hadronic interactions models beyond collider energies*, *Phys. Rev. D* **59**, 094003 (1999) doi:10.1103/PhysRevD.59.094003 [hep-ph/9810384].
- [71] P. Gondolo, G. Ingelman and M. Thunman, *Charm production and high-energy atmospheric muon and neutrino fluxes*, *Astropart. Phys.* **5**, 309 (1996) doi:10.1016/0927-6505(96)00033-3 [hep-ph/9505417].
- [72] L. Anchordoqui, M. T. Dova, A. G. Mariazzi, T. McCauley, T. C. Paul, S. Reucroft and J. Swain, *High energy physics in the atmosphere: Phenomenology of cosmic ray air showers*, *Annals Phys.* **314**, 145 (2004) doi:10.1016/j.aop.2004.07.003 [hep-ph/0407020].
- [73] R. Ulrich, R. Engel and M. Unger, *Phys. Rev. D* **83**, 054026 (2011) doi:10.1103/PhysRevD.83.054026 [arXiv:1010.4310 [hep-ph]].
- [74] M. G. Aartsen *et al.* [IceCube Collaboration], *First observation of PeV-energy neutrinos with IceCube*, *Phys. Rev. Lett.* **111**, 021103 (2013) doi:10.1103/PhysRevLett.111.021103

- [arXiv:1304.5356 [astro-ph.HE]].
- [75] M. G. Aartsen *et al.* [IceCube Collaboration], [Evidence for high-energy extraterrestrial neutrinos at the IceCube detector](#), *Science* **342**, 1242856 (2013) doi:10.1126/science.1242856 [arXiv:1311.5238 [astro-ph.HE]].
- [76] M. G. Aartsen *et al.* [IceCube Collaboration], [Atmospheric and astrophysical neutrinos above 1 TeV interacting in IceCube](#), *Phys. Rev. D* **91**, 022001 (2015) doi:10.1103/PhysRevD.91.022001 [arXiv:1410.1749 [astro-ph.HE]].
- [77] M. G. Aartsen *et al.* [IceCube Collaboration], [Observation of high-energy astrophysical neutrinos in three years of IceCube data](#), *Phys. Rev. Lett.* **113**, 101101 (2014) doi:10.1103/PhysRevLett.113.101101 [arXiv:1405.5303 [astro-ph.HE]].
- [78] M. G. Aartsen *et al.* [IceCube Collaboration], [The IceCube neutrino observatory - Contributions to ICRC 2015 Part II: Atmospheric and astrophysical diffuse neutrino searches of all flavors](#), arXiv:1510.05223 [astro-ph.HE].
- [79] T. K. Gaisser, F. Halzen and T. Stanev, [Particle astrophysics with high-energy neutrinos](#), *Phys. Rept.* **258**, 173 (1995) Erratum: [*Phys. Rept.* **271**, 355 (1996)] doi:10.1016/0370-1573(95)00003-Y [hep-ph/9410384].
- [80] J. G. Learned and K. Mannheim, [High-energy neutrino astrophysics](#), *Ann. Rev. Nucl. Part. Sci.* **50**, 679 (2000). doi:10.1146/annurev.nucl.50.1.679
- [81] F. Halzen and D. Hooper, [High-energy neutrino astronomy: The Cosmic ray connection](#), *Rept. Prog. Phys.* **65**, 1025 (2002) doi:10.1088/0034-4885/65/7/201 [astro-ph/0204527].
- [82] L. A. Anchordoqui and T. Montaruli, [In search for extraterrestrial high energy neutrinos](#), *Ann. Rev. Nucl. Part. Sci.* **60**, 129 (2010) doi:10.1146/annurev.nucl.012809.104551 [arXiv:0912.1035 [astro-ph.HE]].
- [83] L. A. Anchordoqui *et al.*, [Cosmic neutrino pevatrons: A brand new pathway to astronomy, astrophysics, and particle physics](#), *JHEAp* **1-2**, 1 (2014) doi:10.1016/j.jheap.2014.01.001 [arXiv:1312.6587 [astro-ph.HE]].
- [84] M. G. Aartsen *et al.* [IceCube and Pierre Auger and Telescope Array Collaborations], [Search for correlations between the arrival directions of IceCube neutrino events and ultrahigh-energy cosmic rays detected by the Pierre Auger Observatory and the Telescope Array](#), *JCAP* **1601**, no. 01, 037 (2016) doi:10.1088/1475-7516/2016/01/037 [arXiv:1511.09408 [astro-ph.HE]].
- [85] K. Fang, T. Fujii, T. Linden and A. V. Olinto, [Is the ultra-high energy cosmic-ray excess observed by the Telescope Array correlated with IceCube neutrinos?](#), *Astrophys. J.* **794**, no. 2, 126 (2014) doi:10.1088/0004-637X/794/2/126 [arXiv:1404.6237 [astro-ph.HE]].
- [86] M. C. Gonzalez-Garcia and M. Maltoni, [Phenomenology with massive neutrinos](#), *Phys. Rept.* **460**, 1 (2008) doi:10.1016/j.physrep.2007.12.004 [arXiv:0704.1800 [hep-ph]].
- [87] M. G. Aartsen *et al.* [IceCube Collaboration], [Flavor ratio of astrophysical neutrinos above 35 TeV in IceCube](#), *Phys. Rev. Lett.* **114**, 171102 (2015) doi:10.1103/PhysRevLett.114.171102 [arXiv:1502.03376 [astro-ph.HE]].
- [88] S. Palomares-Ruiz, A. C. Vincent and O. Mena, [Spectral analysis of the high-energy IceCube neutrinos](#), *Phys. Rev. D* **91**, 103008 (2015) doi:10.1103/PhysRevD.91.103008 [arXiv:1502.02649 [astro-ph.HE]].
- [89] J. G. Learned and S. Pakvasa, [Detecting tau-neutrino oscillations at PeV energies](#), *Astropart. Phys.* **3**, 267 (1995) doi:10.1016/0927-6505(94)00043-3 [hep-ph/9405296, hep-ph/9408296].

- [90] D. Xu [for the IceCube Collaboration], [Search for astrophysical tau neutrinos with IceCube](#), arXiv:1702.05238 [astro-ph.HE].
- [91] D. Fargion, [Discovering ultra high energy neutrinos by horizontal and upward tau air-showers: Evidences in terrestrial gamma flashes?](#), *Astrophys. J.* **570**, 909 (2002) doi:10.1086/339772 [astro-ph/0002453].
- [92] J. L. Feng, P. Fisher, F. Wilczek and T. M. Yu, [Observability of earth skimming ultrahigh-energy neutrinos](#), *Phys. Rev. Lett.* **88**, 161102 (2002) doi:10.1103/PhysRevLett.88.161102 [hep-ph/0105067].
- [93] X. Bertou, P. Billoir, O. Deligny, C. Lachaud and A. Letessier-Selvon, [Tau neutrinos in the Auger Observatory: A new window to UHECR sources](#), *Astropart. Phys.* **17**, 183 (2002) doi:10.1016/S0927-6505(01)00147-5 [astro-ph/0104452].
- [94] M. Ackermann *et al.* [Fermi-LAT Collaboration], [The spectrum of isotropic diffuse gamma-ray emission between 100 MeV and 820 GeV](#), *Astrophys. J.* **799**, 86 (2015) doi:10.1088/0004-637X/799/1/86 [arXiv:1410.3696 [astro-ph.HE]].
- [95] M. Ackermann *et al.* [Fermi-LAT Collaboration], [Resolving the extragalactic \$\gamma\$ -ray background above 50 GeV with the Fermi Large Area Telescope](#), *Phys. Rev. Lett.* **116**, no. 15, 151105 (2016) doi:10.1103/PhysRevLett.116.151105 [arXiv:1511.00693 [astro-ph.CO]].
- [96] D. Kang *et al.*, [A limit on the diffuse gamma-rays measured with KASCADE-Grande](#), *J. Phys. Conf. Ser.* **632**, no. 1, 012013 (2015). doi:10.1088/1742-6596/632/1/012013
- [97] A. Aab *et al.* [Pierre Auger Collaboration], [The Pierre Auger Observatory: Contributions to the 34th International Cosmic Ray Conference \(ICRC 2015\)](#), arXiv:1509.03732 [astro-ph.HE].
- [98] A. Aab *et al.* [Pierre Auger Collaboration], [Search for photons with energies above \$10^{18}\$ eV using the hybrid detector of the Pierre Auger Observatory](#), [arXiv:1612.01517 [astro-ph.HE]].
- [99] J. Alvarez-Muniz, L. Cazon, R. Conceicao, J. D. de Deus, C. Pajares and M. Pimenta, [Muon production and string percolation effects in cosmic rays at the highest energies](#), arXiv:1209.6474 [hep-ph].
- [100] G. R. Farrar and J. D. Allen, [A new physical phenomenon in ultra-high energy collisions](#), *EPJ Web Conf.* **53**, 07007 (2013) doi:10.1051/epjconf/20135307007 [arXiv:1307.2322 [hep-ph]].
- [101] L. A. Anchordoqui, H. Goldberg and T. J. Weiler, [Strange fireball as an explanation of the muon excess in Auger data](#), *Phys. Rev. D* **95**, no. 6, 063005 (2017) doi:10.1103/PhysRevD.95.063005 [arXiv:1612.07328 [hep-ph]].
- [102] G. Tomar, [Lorentz invariance violation as an explanation of muon excess in Auger data](#), arXiv:1701.05890 [hep-ph].
- [103] Y. A. Fomin, N. N. Kalmykov, I. S. Karpikov, G. V. Kulikov, M. Y. Kuznetsov, G. I. Rubtsov, V. P. Sulakov and S. V. Troitsky, [No muon excess in extensive air showers at 100-500 PeV primary energy: EAS-MSU results](#), arXiv:1609.05764 [astro-ph.HE].
- [104] T. Abu-Zayyad *et al.* [HiRes and MIA Collaborations], [Evidence for changing of cosmic ray composition between \$10^{17}\$ -eV and \$10^{18}\$ -eV from multicomponent measurements](#), *Phys. Rev. Lett.* **84**, 4276 (2000) doi:10.1103/PhysRevLett.84.4276 [astro-ph/9911144].
- [105] A. Haungs [for the KASCADE-Grande Collaboration], [KASCADE-Grande: Composition and post-LHC models](#), talk given at the 19th International Symposium on Very High Energy Cosmic Ray Interactions, Moskow, Russia, August 22-27, 2016.
- [106] V. S. Berezhinsky and G. T. Zatsepin, [Cosmic rays at ultrahigh-energies \(neutrino?\)](#), *Phys.*

- Lett. **28B**, 423 (1969). doi:10.1016/0370-2693(69)90341-4
- [107] F. W. Stecker, **Diffuse fluxes of cosmic high-energy neutrinos**, *Astrophys. J.* **228**, 919 (1979). doi:10.1086/156919
- [108] K. Kotera, D. Allard and A. V. Olinto, **Cosmogenic neutrinos: parameter space and detectability from PeV to ZeV**, *JCAP* **1010**, 013 (2010) doi:10.1088/1475-7516/2010/10/013 [arXiv:1009.1382 [astro-ph.HE]].
- [109] M. Ahlers, L. A. Anchordoqui, M. C. Gonzalez-Garcia, F. Halzen and S. Sarkar, **GZK neutrinos after the *Fermi*-LAT diffuse photon flux measurement**, *Astropart. Phys.* **34**, 106 (2010) doi:10.1016/j.astropartphys.2010.06.003 [arXiv:1005.2620 [astro-ph.HE]].
- [110] R. Aloisio, D. Boncioli, A. di Matteo, A. F. Grillo, S. Petrer and F. Salamida, **Cosmogenic neutrinos and ultrahigh-energy cosmic ray models**, *JCAP* **1510**, no. 10, 006 (2015) doi:10.1088/1475-7516/2015/10/006 [arXiv:1505.04020 [astro-ph.HE]].
- [111] A. Aab *et al.* [Pierre Auger Collaboration], **Improved limit to the diffuse flux of ultrahigh energy neutrinos from the Pierre Auger Observatory**, *Phys. Rev. D* **91**, no. 9, 092008 (2015) doi:10.1103/PhysRevD.91.092008 [arXiv:1504.05397 [astro-ph.HE]].
- [112] P. W. Gorham *et al.* [ANITA Collaboration], **Observational constraints on the ultrahigh-energy cosmic neutrino flux from the second flight of the ANITA experiment**, *Phys. Rev. D* **82**, 022004 (2010) Erratum: [*Phys. Rev. D* **85**, 049901 (2012)] doi:10.1103/PhysRevD.82.022004, 10.1103/PhysRevD.85.049901 [arXiv:1011.5004 [astro-ph.HE]].
- [113] G. Decerprit and D. Allard, **Constraints on the origin of ultrahigh energy cosmic rays from cosmogenic neutrinos and photons**, *Astron. Astrophys.* **535**, A66 (2011) doi:10.1051/0004-6361/201117673 [arXiv:1107.3722 [astro-ph.HE]].
- [114] V. Kuzmin and I. Tkachev, **Ultrahigh-energy cosmic rays, superheavy long living particles, and matter creation after inflation**, *JETP Lett.* **68**, 271 (1998) [*Pisma Zh. Eksp. Teor. Fiz.* **68**, 255 (1998)] doi:10.1134/1.567858 [hep-ph/9802304].
- [115] S. L. Dubovsky and P. G. Tinyakov, **Galactic anisotropy as signature of CDM related ultrahigh-energy cosmic rays**, *JETP Lett.* **68**, 107 (1998) doi:10.1134/1.567830 [hep-ph/9802382].
- [116] V. Berezhinsky and M. Kachelriess, **Limiting SUSY QCD spectrum and its application for decays of superheavy particles**, *Phys. Lett. B* **434**, 61 (1998) doi:10.1016/S0370-2693(98)00728-X [hep-ph/9803500].
- [117] M. Birkel and S. Sarkar, **Extremely high-energy cosmic rays from relic particle decays**, *Astropart. Phys.* **9**, 297 (1998) doi:10.1016/S0927-6505(98)00028-0 [hep-ph/9804285].
- [118] P. Blasi, R. Dick and E. W. Kolb, **Ultrahigh-energy cosmic rays from annihilation of superheavy dark matter**, *Astropart. Phys.* **18**, 57 (2002) doi:10.1016/S0927-6505(02)00113-5 [astro-ph/0105232].
- [119] S. Sarkar and R. Toldra, **The high-energy cosmic ray spectrum from relic particle decay**, *Nucl. Phys. B* **621**, 495 (2002) doi:10.1016/S0550-3213(01)00565-X [hep-ph/0108098].
- [120] R. Aloisio, S. Matarrese and A. V. Olinto, **Super heavy dark matter in light of BICEP2, Planck and ultrahigh energy cosmic ray observations**, *JCAP* **1508**, no. 08, 024 (2015) doi:10.1088/1475-7516/2015/08/024 [arXiv:1504.01319 [astro-ph.HE]].
- [121] C. A. Kierans *et al.*, **The 2016 Super Pressure Balloon flight of the Compton Spectrometer and Imager**, arXiv:1701.05558 [astro-ph.IM].

- [122] J. H. Adams, Jr. *et al.*, [Summary Report of JEM-EUSO Workshop at KICP in Chicago](#), arXiv:1203.3451 [astro-ph.IM].
- [123] T. Bergmann, R. Engel, D. Heck, N. N. Kalmykov, S. Ostapchenko, T. Pierog, T. Thouw and K. Werner, [One-dimensional hybrid approach to extensive air shower simulation](#), *Astropart. Phys.* **26**, 420 (2007) doi:10.1016/j.astropartphys.2006.08.005 [astro-ph/0606564].
- [124] <http://www.zemax.com>
- [125] E. J. Schioppa *et al.*, [The SST-1M camera for the Cherenkov Telescope Array](#), *PoS ICRC 2015*, 930 (2016) [arXiv:1508.06453 [astro-ph.IM]].
- [126] S. Argiro, S. L. C. Barroso, J. Gonzalez, L. Nellen, T. C. Paul, T. A. Porter, L. Prado, Jr. and M. Roth, R. Ulrich, and D. Veberič, [The Offline software framework of the Pierre Auger Observatory](#), *Nucl. Instrum. Meth. A* **580**, 1485 (2007) doi:10.1016/j.nima.2007.07.010 [arXiv:0707.1652 [astro-ph]].
- [127] P. Abreu *et al.* [Pierre Auger Collaboration], [Advanced functionality for radio analysis in the Offline software framework of the Pierre Auger Observatory](#), *Nucl. Instrum. Meth. A* **635**, 92 (2011) doi:10.1016/j.nima.2011.01.049 [arXiv:1101.4473 [astro-ph.IM]].
- [128] C. Berat *et al.*, [ESAF: Full simulation of space-based extensive air showers detectors](#), *Astropart. Phys.* **33**, 221 (2010) doi:10.1016/j.astropartphys.2010.02.005 [arXiv:0907.5275 [astro-ph.IM]].
- [129] A. Aab *et al.* [Pierre Auger Collaboration], [The Pierre Auger cosmic ray observatory](#), *Nucl. Instrum. Meth. A* **798**, 172 (2015) doi:10.1016/j.nima.2015.06.058 [arXiv:1502.01323 [astro-ph.IM]].
- [130] B. Boehm, [Software engineering economics](#), Englewood Cliffs, NJ:Prentice-Hall, 1981. ISBN 0-13-822122-7.
- [131] M. Bohacova *et al.* [AIRFLY Collaboration], [A novel method for the absolute fluorescence yield measurement by AIRFLY](#), *Nucl. Instrum. Meth. A* **597**, 55 (2008) doi:10.1016/j.nima.2008.08.049 [arXiv:0812.3649 [astro-ph]].
- [132] S. J. Sciutto, [AIRES: A System for air shower simulations](#), astro-ph/9911331.
- [133] D. Heck, G. Schatz, T. Thouw, J. Knapp and J. N. Capdevielle, [CORSIKA: A Monte Carlo code to simulate extensive air showers](#), FZKA-6019.
- [134] H. J. Drescher and G. R. Farrar, [Air shower simulations in a hybrid approach using cascade equations](#), *Phys. Rev. D* **67**, 116001 (2003) doi:10.1103/PhysRevD.67.116001 [astro-ph/0212018].
- [135] <https://geant4.cern.ch>
- [136] D. Ardouin *et al.*, [CODALEMA: A cosmic ray air shower radio detection experiment](#), *Int. J. Mod. Phys. A* **21S1**, 192 (2006). doi:10.1142/S0217751X0603360X
- [137] B. A. Antokhonov *et al.*, [A new 1-km² EAS Cherenkov array in the Tunka valley](#), *Nucl. Instrum. Meth. A* **639**, 42 (2011). doi:10.1016/j.nima.2010.09.142
- [138] A. U. Abeysekara *et al.* [HAWC Collaboration], [The HAWC gamma-ray observatory: Design, calibration, and operation](#), arXiv:1310.0074 [astro-ph.IM].
- [139] <http://www.lofar.org/>
- [140] O. Wyszynski, A. Laszlo, A. Marcinek, T. Paul, R. Sipos, M. Szuba, M. Unger and D. Veberič, [Legacy code: Lessons from NA61/SHINE offline software upgrade adventure](#), *J. Phys. Conf. Ser.* **396**, 052076 (2012). doi:10.1088/1742-6596/396/5/052076

- [141] R. Sipos, A. Laszlo, A. Marcinek, T. Paul, M. Szuba, M. Unger, D. Veberić and O. Wyszynski, *The offline software framework of the NA61/SHINE experiment*, J. Phys. Conf. Ser. **396**, 022045 (2012). doi:10.1088/1742-6596/396/2/022045
- [142] <http://www.opensource.org/>
- [143] <http://root.cern.ch/>
- [144] D. Naumov, *SLAST, Shower Light Attenuated to the Space Telescope*, EUSO mission internal document (2003).
- [145] National Oceanic Atmospheric Administration et al., *U.S standard atmosphere, 1976*, public document (1976).
- [146] M. Nagano, K. Kobayakawa, N. Sakaki and K. Ando, *New measurement on photon yields from air and the application to the energy estimation of primary cosmic rays*, Astropart. Phys. **22**, 235 (2004) doi:10.1016/j.astropartphys.2004.08.002 [astro-ph/0406474].
- [147] F. Kakimoto, E. C. Loh, M. Nagano, H. Okuno, M. Teshima and S. Ueno, *A measurement of the air fluorescence yield*, Nucl. Instrum. Meth. A **372**, 527 (1996). doi:10.1016/0168-9002(95)01423-3
- [148] Air Force Geophysics Laboratory, *Users guide to LOWTRAN 7*, public document (1988).
- [149] <http://xerces.apache.org/>
- [150] <http://www.w3.org/standards/xml/schema>
- [151] <http://sourceforge.net/projects/cppunit/>
- [152] <http://buildbot.net/>
- [153] <http://www.cmake.org>
- [154] <https://svn.auger.unam.mx/trac/projects/ape/>
- [155] P. V. Ballmoos, *The EUSO-BALLOON mission*, PoS ICRC **2015**, 322 (2016).
- [156] L. W. Piotrowski *et al.*, *On-line and off-line data analysis for the EUSO-TA experiment*, Nucl. Instrum. Meth. A **773**, 164 (2015). doi:10.1016/j.nima.2014.08.045
- [157] F. Bisconti [JEM-EUSO Collaboration], *EUSO-TA fluorescence detector*, arXiv:1701.07091 [astro-ph.IM].
- [158] M. Ricci, *Mini-EUSO: a pathfinder for JEM-EUSO to measure Earths UV background from the ISS*, PoS ICRC **2015**, 599 (2016).
- [159] L. Wiencke, *EUSO-Balloon mission to record extensive air showers from near space*, PoS ICRC **2015**, 631 (2016).
- [160] S. Cambursano *A simulation study of the EUSO-SPB trigger and reconstruction performances*, MSc Dissertation, Torino University (2016).
- [161] A. Veneziani, *Study on the expected sky conditions during Super Pressure Balloon flights and observation of cosmic rays*, Bachelor Thesis, Torino University (2016)
- [162] E. Bertola, *Study on the response of the Mini-EUSO first trigger level* Bachelor Thesis, Torino University (2016).
- [163] L. A. Anchordoqui, K. Islo, A. V. Olinto, T. C. Paul, and B. Vlcek, *Cosmic neutrino detection from the International Space Station*, XXVI International Conference on Neutrino Physics and Astrophysics (Neutrino 2014), Boston, June 2-7, 2014. <http://neutrino2014.bu.edu/files/2013/08/Neutrino-2014-Poster-contributions-book.pdf>
- [164] D. Lorenz, *Dark Site Finder*, <http://darksitefinder.com/map/>.

- [165] G. Sáez-Cano *et al.* [JEM-EUSO Collaboration], **Observation of ultra-high energy cosmic rays in cloudy conditions by the JEM-EUSO Space Observatory**, doi:10.7529/ICRC2011/V03/1034
- [166] A. Guzman *et al.* [JEM-EUSO Collaboration], **The JEM-EUSO observation in cloudy conditions**, *Exper. Astron.* **40**, no. 1, 135 (2015). doi:10.1007/s10686-014-9377-2
- [167] G. Sáez-Cano *et al.* [JEM-EUSO Collaboration], **Observation of ultra-high energy cosmic rays in cloudy conditions by the space-based JEM-EUSO Observatory**, *J. Phys. Conf. Ser.* **375**, 052010 (2012). doi:10.1088/1742-6596/375/1/052010
- [168] G. Sáez-Cano *et al.* [JEM-EUSO Collaboration], **Observation of extensive air showers in cloudy conditions by the JEM-EUSO Space Mission**, *Adv. Space Res.* **53**, 1536 (2014). doi:10.1016/j.asr.2013.07.015
- [169] A. Cummings, **Field testing for extreme universe space observatory aboard a super pressure balloon (EUSO-SPB): Logistics and first results**, MSc Dissertation, Colorado School of Mines (2017).
- [170] J. S. Fenn, **Estimating the cosmic ray extensive air shower detection rate for the EUSO Super Pressure Balloon mission**, MSc Dissertation, Colorado School of Mines (2015). <http://hdl.handle.net/11124/17150>